Transitions in cell potency during early mouse development are driven by Notch

Sergio Menchero[1], Antonio Lopez-Izquierdo[1], Isabel Rollan[1], Julio Sainz de Aja[1, †], Maria Jose Andreu[1], Minjung Kang[2], Javier Adan[1], Rui Benedito[3], Teresa Rayon[1, †], Anna-Katerina Hadjantonakis[2] and Miguel Manzanares[1,*]

[1] Centro Nacional de Investigaciones Cardiovasculares Carlos III (CNIC), Melchor Fernández Almagro 3, 28029 Madrid, Spain.

[2] Developmental Biology Program, Sloan Kettering Institute, New York NY 10065, USA.

[3] Molecular Genetics of Angiogenesis Group, Centro Nacional de Investigaciones Cardiovasculares Carlos III (CNIC), Melchor Fernández Almagro 3, 28029 Madrid, Spain.

[†] Current address: Children's Hospital, Stem Cell Program, 300 Longwood Ave, Boston MA 02115, USA.

[†] Current address: The Francis Crick Institute, 1 Midland Road, London NW1 1AT, UK.

* Corresponding author (mmanzanares@cnic.es)

Abstract

The Notch signalling pathway plays fundamental roles in diverse developmental processes in metazoans, where it is important in driving cell fate and directing differentiation of various cell types. However, we still have limited knowledge about the role of Notch in early preimplantation stages of mammalian development, or how it interacts with other signalling pathways active at these stages such as Hippo. By using genetic and pharmacological tools in vivo, together with image analysis of single embryos and pluripotent cell culture, we have found that Notch is active from the 4-cell stage. Transcriptomic analysis in single morula identified novel Notch targets, such as early naïve pluripotency markers or transcriptional repressors such as TLE4. Our results reveal a previously undescribed role for Notch in driving transitions during the gradual loss of potency that takes place in the early mouse embryo prior to the first lineage decisions.

Introduction

The totipotent mammalian zygote has the self-organising capacity of generating embryonic and extraembryonic structures to build a complete organism [1]. This undifferentiated cell will proliferate and its descendants will take lineage decisions that entail a progressive loss of potency. The first differentiation event that leads to distinct lineages takes place during preimplantation development at the morula to blastocyst transition, resulting in the formation of the trophectoderm (TE, extraembryonic population) and the inner cell mass (ICM, embryonic population). How the establishment of these early lineages is achieved has been widely studied and we now know that a combination of morphogenetic cues breaks the symmetry in the embryo [2–4]. The first morphological sign of differentiation is evident in the compacting morula, 2.5 days after fertilization (embryonic day E2.5), when blastomeres increase their intercellular interactions and outer cells acquire an apical-basal polarity. These polarized cells on the surface enclose an inner group of apolar cells [5,6]. The outer versus inner position of the blastomeres correlates with their fate, becoming TE or ICM respectively, although cells can change their position within the embryo [7–9]. Prior to compaction, blastomeres appear morphologically equivalent. However, transcriptional differences among blastomeres have been described as early as in the 4-cell embryo [10–12]. Although cells at this stage are not committed to a specific fate, these early heterogeneities correlate with specific fate biases before lineage commitment. However, how these early heterogeneities arise and their implications in cell plasticity are still unclear [13].

Once the embryo compacts, differences in contractility and the activity of signalling pathways orchestrate the lineage-commitment of cell populations [14–20]. The initial stochastic expression of the main lineage-specific transcription factors (such as CDX2 or GATA3 for the TE, and OCT4 or NANOG for the ICM) is gradually restricted to their definitive domains [21,22]. The Hippo pathway has been shown to act as a readout of

cell polarity and therefore, differential intercellular distribution of its components and thus differential activity in polar or apolar cells, will dictate fate [23–26]. In outer cells, the pathway is switched off and the transcriptional coactivator YAP is translocated to the nucleus where it will interact with TEAD4, the effector of the pathway, to promote the expression of key TE genes such as *Cdx2* and *Gata3* [15,27]. We have previously shown that Notch signalling also has a role in the regulation of *Cdx2*. It is specifically active in the TE, where the intracellular domain of the Notch receptor (NICD) is translocated into the nucleus where it binds to the transcription factor RBPJ to promote target gene expression. Both Notch and Hippo converge on the TEE, an enhancer upstream of *Cdx2* [16]. YAP/TEAD and NICD/RBPJ transcriptional complexes interact with the chromatin modifier SBNO1 to favour the induction of *Cdx2* [28].

Nevertheless, we still do not understand how these two signalling pathway interact to regulate *Cdx2* in the embryo, if there is crosstalk between them, if they are acting in parallel during development or otherwise. Furthermore, Notch signalling could have other unexplored roles at early stages of mouse development. In this study, we show that Hippo and Notch pathways are largely independent, but that Notch is active earlier, before compaction, and that differences in Notch levels determines cell fate in the blastocyst. Single-embryo RNA-seq points at repressors that block early naïve pluripotency markers as Notch targets. We propose that Notch coordinates the triggering of initial differentiation events within the embryo and regulates the early specification of the trophectoderm.

Results

CDX2 expression in the morula is dependent on the Notch and Hippo signalling pathways.

Previously, we have described how Notch and Hippo pathways converge to regulate *Cdx2* expression, and that different allelic combinations for *Rbpj* and *Tead4* lead to a significantly reduced expression of CDX2 [16]. Notably, we failed to recover double mutant embryos at the blastocyst stage (E3.5), suggesting that the lack of both factors caused lethality before the blastocyst stage. We therefore decided to investigate embryos at the earlier morula stage (E2.5), where we recovered double mutant embryos at Mendelian ratios. CDX2 levels were lower in *Rbpj*$^{-/-}$;*Tead4*$^{+/-}$ and *Rbpj*$^{+/-}$;*Tead4*$^{-/-}$ morulae, as previously observed in blastocysts [16]. Interestingly, this effect was exacerbated in double mutant embryos (*Rbpj*$^{-/-}$;*Tead4*$^{-/-}$) in which we did not detect any CDX2 expression, although OCT4 was normally expressed (Fig 1A).

Compaction of blastomeres and polarization of outer cells are critical morphological events that take place at the morula stage and are linked to the onset of CDX2 expression [29,30]. We therefore decided to investigate if these processes were affected in double mutant morulae. We examined the expression of E-cadherin and phospho-ERM, as markers of cell-cell adhesion and apical polarity. No differences in the distribution or intensity of these markers was observed in any of the allelic combinations examined, including double mutants for *Rbpj* and *Tead4* (Fig S1). Therefore, disruption of Notch and Hippo signalling does not alter cellular and morphological events prior to lineage specification, but does result in a dramatic downregulation of *Cdx2* at this stage.

To better understand the contributions of each of the Notch and Hippo pathways to CDX2 expression, we performed correlations in single cells between Notch, YAP and CDX2. We used a transgenic mouse line carrying CBF1-VENUS as a reporter of Notch

activity [31], and we performed immunostaining to detect YAP and CDX2 in morulae and blastocysts from that reporter line. In the blastocyst, the three markers were restricted to nuclei of the TE, while in the morula their expression was more heterogeneous (Fig 1B). Nuclear YAP was detected preferentially in outer cells, presumably polarized blastomeres, whereas CBF1-VENUS and CDX2 were detected in both inner and outer cells of the morula. We quantified nuclear intensity levels using a Matlab based segmentation tool, MINS [32], and found that CBF1-VENUS and YAP both correlated positively with CDX2 at morula and blastocyst stages (Fig 1C and 1D, respectively). Interestingly, there was no correlation between CBF1-VENUS and YAP in the morula, suggesting that the two pathways are activated independently at this stage (Fig 1C). By the blastocyst stage, these markers did show a positive correlation, albeit weaker than the correlation of either marker with CDX2 (Fig 1D). If all three components were taken into account simultaneously, the coefficient of correlation increases both in morula (Fig 1E) and blastocyst (Fig 1F), indicating that the combination of Notch and Hippo pathways better accounted for CDX2 levels than any of them individually.

In most cases, individual nuclei from morulae were positive for the three markers. However, we did find a few cases in which nuclei were positive for CBF1-VENUS and CDX2 but negative for YAP (Fig 1B, arrowhead). We therefore analysed all morulae to determine the distribution of cells positive for each combination of markers. We found that Notch was active in most of the cells at this stage and that the majority of blastomeres were positive for all three of the markers (295 blastomeres, 72.3%; Fig 1G). Another noteworthy population was represented by cells that were only positive for CBF1-VENUS and CDX2 (85 blastomeres, 20.8%). However, we rarely found cells expressing YAP and CDX2 but not CBF1-VENUS at the morula stage (Fig 1G). Together, this set of experiments shows that Notch and Hippo are responsible for

CDX2 expression at the morula stage, and suggests that they are generally acting in an independent fashion.

Absence of crosstalk between the Notch and Hippo signalling pathways in the early mouse embryo.

The correlation analysis between CBF1-VENUS and YAP expressing blastomeres indicated possible independent roles for Notch and Hippo in the regulation of CDX2 expression (Fig 1C). Furthermore, our previous results showed how these two pathways acted in parallel to transcriptionally regulate *Cdx2* through a distal enhancer element [16]. To further study the interaction between these pathways, we examined TEAD4 and YAP expression in *Rbpj*$^{-/-}$ (Fig S2A and S2B) and *Notch1*$^{-/-}$ (Fig S2C and S2D) blastocysts. We did not detect any differences in levels or pattern of expression of TEAD4 and YAP either in *Rbpj*$^{-/-}$ or in *Notch1*$^{-/-}$ embryos as compared to wildtype embryos. We also studied the reverse situation, crossing the CBF1-VENUS mouse line as a reporter of Notch pathway activity into the *Tead4* null background. We detected VENUS fluorescent protein in both wildtype and *Tead4*$^{-/-}$ embryos (Fig S2E). Interestingly, CBF1-VENUS expression was maintained in outer cells although the *Tead4*$^{-/-}$ embryos do not form a proper blastocyst [33], suggesting that some degree of outer identity still is present in *Tead4*$^{-/-}$ embryos. These results confirm that Notch is not required for proper deployment of the transcriptional effectors of the Hippo pathway, and vice versa, that activation of the Notch pathway can occur in the absence of YAP/TEAD4 activity.

Given that the Hippo pathway is the major regulator of *Cdx2* expression, we wanted to assess if forced activation of the Notch pathway would be sufficient to compensate and restore *Cdx2* wildtype levels in a *Tead4* null background. To do this, we crossed the *Tead4* null allele with a mouse line that conditionally overexpresses the active

intracellular domain of the Notch1 receptor (N1ICD) with a GFP reporter under the Rosa26 promoter (Rosa26-stop-N1ICD-ires-eGFP) [34], and used a mouse line carrying a maternal *Sox2*-Cre allele to recombine it in oocytes [35]. Although there is a certain degree of mosaicism in embryos from this cross (mean of 87% of GFP+ cells in recombined blastocysts), we observed a significant increase in CDX2 intensity levels in *N1ICD-GFP*;*Tead4*$^{-/-}$ embryos as compared to *Tead4*$^{-/-}$ embryos (Fig S2F and S2G). However, this was not sufficient to rescue the *Tead4*$^{-/-}$ phenotype, as *N1ICD-GFP*;*Tead4*$^{-/-}$ embryos still fail to form a blastocyst (Fig S2F). Thus, both pathways are acting independently of each other, and while Notch is able to positively regulate *Cdx2* in the absence of TEAD4 transcriptional activity, it is not sufficient on its own to rescue its loss.

Notch regulates the onset of *Cdx2* expression.

To better understand how parallel signalling pathways drive *Cdx2* expression, we determined if the temporal expression of *Cdx2* was regulated differentially by Notch and Hippo. To do so, we took advantage of pharmacological compounds that allow inhibition of these pathways in a time-controlled manner. We used RO4929097 (RO) to inhibit the Notch pathway [36] and Verteporfin to block the YAP-TEAD4 interaction [37]. We treated wildtype embryos in two different time-windows: from the two-cell up to morula stage, and from morula to blastocyst. As a control, we treated embryos with DMSO, the solvent used for diluting both inhibitors. After treatment, gene expression in embryos was analysed by RT-qPCR. In the early time window, from two-cell to morula, we observed that *Cdx2* was downregulated when Notch was inhibited, while there was no change when Hippo pathway activity was altered (Fig 2A). Interestingly, the opposite was found when we modulated the pathways from the morula onwards. *Cdx2* expression was only affected when YAP-TEAD4 activity was blocked (Fig 2B). These results show that, although both pathways cooperate in the regulation of *Cdx2*, they act

sequentially to regulate *Cdx2* levels in a stage specific manner rather than being redundant. *Gata3*, *Oct4* and *Nanog* were not significantly changed after Notch or YAP inhibition in any of the time windows, indicating that *Cdx2* is the main target of the pathways.

Next, we wished to confirm these observations in morula stage embryos using genetic loss of function models. We recovered early (8-16 cells) and late (17-32 cells) morulae and analysed CDX2 expression in wildtype and *Rbpj*$^{-/-}$ embryos (Fig 2C and 2E). We counted CDX2 positive cells in individual embryos and found that *Rbpj*$^{-/-}$ early morulae had a significantly lower number compared to control littermates (Fig 2D). In contrast, we did not observe differences at the late morula stage (Fig 2F). The same observations were obtained when we analysed embryos from another mutant for the pathway, *Notch1*$^{-/-}$: early morulae (8-16 cells) showed a decrease in the number of CDX2 positive cells (Fig S3A and S3B), but late (17-32 cells) morulae did not (Fig S3C and S3D). This result is interesting, as it demonstrates that *Notch1* is the main player of the Notch pathway during preimplantation development and its loss is enough to recapitulate *Rbpj* loss of function effects.

These results indicate that there is an earlier requirement for Notch than for Hippo in the regulation of *Cdx2*, and that both pathways exert non-redundant roles. Our observations are suggestive of a model where Notch regulates the onset of *Cdx2* expression, and the Hippo pathway subsequently maintains its expression.

The Notch pathway is heterogeneously active in the embryo starting at the 4-cell stage.

In light of the above findings revealing a requirement of the Notch pathway for the early stages of mouse preimplantation development, we decided to investigate when Notch is first active, using the CBF1-VENUS reporter line as a transcriptional readout of the

pathway. We recovered embryos from the CBF1-VENUS line and found that the reporter was first active in 4-cell embryos, albeit at lower levels than at later stages (Fig 3A). The number of VENUS positive cells was variable among embryos, with at least a third of embryos examined having no positive cells (7 out of 20; Fig S4A). This strongly suggest that the onset of Notch pathway activation is indeed occurring at this stage. As a general rule, the number of positive blastomeres increased with the total number of cells per embryo (Fig 3B and Fig S4A). In the compacted morula, most of the cells were positive, but the activity of the reporter was quickly restricted to the outer TE cells once the blastocyst formed (Fig 1B).

In order to follow the dynamics of the reporter and determine how restriction of Notch activity is achieved during development, we performed live imaging for up to 24 hours of embryos from the compacted morula (16-cell) to the early blastocyst stage (Movie 1, Fig 3C). After tracking of the cells in each embryo (n=7; Fig S4B), we used a Matlab based tool to analyse the behaviour of each individual cell and its progeny within the embryo. With this tool, we were able to reconstruct the embryo in each time point and assign an initial position (inner or outer) to each blastomere as well as its final location in the TE/out or the ICM/in (Movie 2, Fig 3D). We first generated a lineage tree so that each lineage or family includes a cell in the time frame 0 and all their descendant cells. We next classified families according to the position of the cells in the first and final time points. This allowed us to divide the cells in four groups: “IN-ICM” (cells that began in an inner position and their descendants remained in an inner position), “IN-TE+ICM” (cells that began in an inner position and at least one of their descendants ended up in an inner position but other/s in an outer position), “OUT-TE” (cells that began in an outer position and their descendants remained in an outer position), and “OUT-TE+ICM” (cells that began in an outer position and at least one of their descendants ended up in an outer position but other/s ended up in an inner position).

Confirming previous findings [8,9,22,38,39], although most of the cells of the blastocyst retain the position of their predecessor cell in the compacted morula, a small percentage change their location (Fig S4C). We next measured intensity levels of the reporter in all cells within families, and determined if it correlated with their position during the time lapse. Notch activity levels were variable among families and embryos, but we detected higher and increasing levels in OUT-TE families while IN-ICM families generally showed lower and decreasing levels (Fig S4D and S4E). The intensity levels in families that contributed both inner and outer cells did not follow a clear pattern (Fig S4F). When we analysed the mean intensity for each group, we saw that VENUS levels were significantly lower in the families that were always inside as compared to the families that were always outside (Fig 3E). Interestingly, this difference was already manifest when we measured the initial intensity in the first time point (Fig 3F). In the families whose cells end up in both inner and outer position, VENUS levels were intermediate (Fig 3E, F).

Therefore, the analysis of the CBF1-VENUS line showed that the reporter is active before the first lineage decision is taken, and that differences in the levels of pathway activation in inner or outer cells of the compacted morula correlate with the final position of their descendants in the blastocyst.

Different Notch levels determines cell position in the morula and the blastocyst.

We have previously shown that increasing the activity of the Notch signalling pathway leads to a preferential allocation of cells to the outer trophectoderm of the blastocyst [16]. However, we had not tested the onset of this effect and whether blocking Notch would have an effect in early embryos. To address these questions, we used a genetic mosaic line (iChr-Notch-Mosaic) that allowed us to generate cells with different Notch

activity levels within the same embryo [40]. The construct consists of three different cassettes preceded by a specific LoxP site. The first cassette is a H2B-CHERRY fluorescent protein and generates wildtype cells. The second cassette contains a dominant-negative version of *Mastermind-like 1* (DN-MAML1), a transcriptional co-activator of the Notch pathway, linked to a H2B-eGFP by a cleavable 2A peptide, whose expression leads to the loss of function (LOF) of the pathway, while the third is a gain of function (GOF) cassette through the expression of a constitutively active NICD linked to an HA-H2B-Cerulean (Fig 4A). The specific LoxP sites are mutually exclusive, so in any unique cell there will be only one possible outcome as the result of Cre-mediated recombination. We used a Polr2a^{CreERT2} driver which is ubiquitously expressed and inducible by tamoxifen [41]. We induced recombination by adding 4OH-Tx (4-hydroxy-tamoxifen) from the 2- to the 4-cell stage, aiming to achieve a situation where cells expressing each cassette derive from a single recombined blastomere, and we evaluated recombination in the late morula (<32 cells) or in the blastocyst (Fig 4A). We performed immunofluorescent assays with three antibodies to distinguish the 3 cassettes. The wildtype cassette was detected by an anti-RFP antibody, the LOF by an anti-GFP antibody, and the GOF an anti-HA antibody. However, GOF cells were triple positive because of cross-reactivity between antibodies and the HA-H2B-Cerulean protein (Fig 4A, B).

We selected embryos in which all three recombination events had occurred and analysed the percentage of cells expressing the control, LOF or GOF cassette. Although the probabilities of recombination are higher when the LoxP sites are closer to one another (the control recombination event in this case), we found that most of the cells (58%) were Notch GOF while only a small proportion (10%) were Notch LOF, suggesting that Notch activity could affect cell proliferation in the embryo (Fig 4C; Fig S5A-B). Next, we determined the proportion of cells from each population that were in an inner or outer position. Approximately 60% of wildtype (red) cells were located at

outer positions in both morula and blastocyst stage. However, Notch-LOF cells (green) were enriched at inner positons of the morula or in the inner cell mas of the blastocyst, while Notch-GOF cells (blue) tended to occupy outer positions (Fig 4D, E). These experiments show how manipulating levels of Notch pathway activity as early as the 4-cell stage instructs cells to adopt an inner or outer position at later stages.

Lack of *Rbpj* represses *Tle4* and *Tbx3*, and disrupts the triggering of differentiation programs in the early embryo.

Results described above show that the Notch pathway plays an early role in mouse development, non-redundant with that of the Hippo pathway, in regulating *Cdx2* gene expression and in determining the position of cells to inner or outer locations. To gain further insight into how Notch is acting during preimplantation development, we carried out RNA-sequencing (RNA-seq) in control and *Rbpj*$^{-/-}$ single morulae, obtained from the same litter to reduce variability. Hierarchical clustering separated the control group (wildtype and heterozygotes) from homozygotes *Rbpj*$^{-/-}$ morulae (Fig S6A). 1273 genes were differentially expressed (Table S1), 79% of which were downregulated suggesting that *Rbpj* is mainly activating gene expression at the morula stage.

Among the downregulated genes we found *Cdx2* and other TE associated genes such as *Gata2*, *Gata3* or *Fgfr2* [27,42–44]; genes related with the Hippo pathway (*Tead4*, *Nf2*, *Lats2*) and, interestingly, also genes related with the embryonic pluripotency network including *Sall1*, *Sall4, Tbx3* or *Sox21* [10,45–48] (Fig 5A, Fig S6B). Among the upregulated genes, we found *Dppa3* (*Stella*) and *Prdm14*, which have been characterised as naïve pluripotency markers [49,50]. In addition, a large set of chromatin modifiers were differentially expressed (Fig S6C). Important chromatin dynamics have been reported during preimplantation development [51], which could fit in with the broad mis-regulation of transcription in the mutant embryos. Remarkably,

some of the downregulated modifiers like *Dnmt3b* or *Kdm6a* have been shown to be enriched in TE conversely to *Prdm14* [12]. Overall, the transcriptome profiling suggests that embryos lacking *Rbpj* do not properly trigger trophectoderm differentiation programs, and that they also affect pluripotency related genes.

To identify direct targets of Notch signalling at this stage, we searched for putative RBPJ binding sites in the vicinity of differentially expressed genes. We established an arbitrary window of 10 Kb surrounding each gene to perform the analysis and found RBPJ binding motifs in 921 genes. We then examined how many of these putative binding sites were located in regions of open chromatin, a hallmark for active regulatory elements. For this, we took advantage of ATAC-seq profiles from published datasets of 8-cell mouse embryos [52], and reduced our list to 186 genes (Fig 5B; Table S2). Among these was *Cdx2*, where the predicted RBPJ sites and ATAC-seq open chromatin signature mapped to the TEE enhancer we had previously characterized [16], thus validating this approach.

We selected two genes as putative Notch targets, that were downregulated in *Rbpj*$^{-/-}$ morulae and had been previously associated with exit from pluripotency in mouse ES cells: those coding for the Groucho-family transcriptional repressor TLE4 [53], and the T-box family transcription factor TBX3 [54,55]. Both genes are heterogeneously expressed in ES cells and repress naïve pluripotency genes. We hypothesized that *Tle4* and *Tbx3* could be direct targets of Notch, and that their downregulation could in part explain the blockade in differentiation that we observe in the RNA-seq. We independently confirmed downregulation of their expression after blocking the Notch pathway by treating wildtype embryos with the RO4929097 inhibitor from 2-cell to morula stage (Fig 5C).

An RBPJ motif search within ATAC-seq peaks in the vicinity of the genes identified two potential candidate regions located 1.3 Kb upstream of *Tle4* (Tle4-up; Fig 5D) and in the seventh intron of *Tbx3* (Tbx3-i7; Fig S6D), respectively. By means of transient

transgenic assays, we proved that these regions could act as transcriptional enhancers driving H2B-mRFP reporter expression in the morula (32% positive embryos for the 700 bp Tle4-up element, Fig 5E; and 56% for the 600 bp Tbx3-i7 element; Fig S6E). To test if Notch was directly involved, we mutated the RBPJ motif inside these regions and found that the activity of the Tle4-up mut^{RBPJ} fragment was significantly diminished (from 32% to 13% positive embryos, Fig 5E, F) while the Tbx3-i7 mut^{RBPJ} fragment was not affected (60% positive embryos, Fig S6E-F). Finally, to examine whether these enhancers were necessary for the expression of their putative target genes, we deleted the regions within the enhancers that contained the RBPJ motif by CRISPR/Cas9 mediated genome editing [56], and analysed gene expression by qPCR on individually edited morulae. We observed a significant decrease in *Tle4* expression in edited embryos (deleted, n=10) as compared to injected embryos that had been partially (mosaic, n=9) or not (wildtype, n=14) edited (Fig 5G). However, *Tbx3* expression did not change when the RBPJ motif from the seventh intron was deleted (Fig S6G). These assays provide evidence that these genomic regions act as *cis*-regulatory elements and, in the case of *Tle4*, are directly regulated by RBPJ and necessary for correct expression.

Notch levels coordinate the balance between naïve pluripotency and triggering of differentiation in ES cells.

The transcriptomic profiling carried out in *Rbpj*$^{-/-}$ embryos identified genes related with naïve pluripotency among the upregulated genes. Naïve pluripotency corresponds to a state in which cells are not prone to differentiate, in contrast to primed pluripotency [57]. These pluripotent states as well as the transition between them have been extensively studied in ES cells and EpiLCs, *in vitro* counterparts of the epiblast of the blastocyst stage preimplantation embryo and the postimplantation pre-gastrulating epiblast respectively [58]. Interestingly, some of these naïve markers such as *Prdm14*

are initially expressed at the 2- and 4-cell stage, switched off in the morula and re-expressed in the ICM of the blastocyst [12]. Analysis of published single-cell RNA-seq data [10] confirmed that *Prdm14* decreased dramatically from the 4-cell to 8-cell stage, and expression of *Dppa3* also decreases from the 2-cell to the 4-cell stage (Fig S7A). In contrast, *Tle4* and *Tbx3* levels increased from the 4- to 8-cell stage (Fig S7A). Our data from *Rbpj*$^{-/-}$ morulae suggests that embryos do not switch off *Prdm14* and *Dppa3*, and inhibiting Notch with RO4929097 from the 2-cell to 4-cell stage confirmed the effect on *Prdm14*, whose levels were significantly increased after the treatment (Fig S7B).

We wondered if the effect of Notch guiding differentiation programs that we had seen in the embryo was also occurring in ES cells. We used iChr-Notch-Mosaic ES cells [40] to confront populations with different Notch levels using the same strategy than we had previously used in the embryo (Fig 6A). After recombination by transfection with *Cre*, ES cells were sorted according to the fluorescent reporter cassette they expressed (Fig 6B). We measured expression levels of naïve pluripotency markers by qPCR, and found that levels of *Prdm14* and *Dppa3* correlated negatively with Notch activity but other markers such as *Nanog* or *Esrrb* were not altered (Fig 6C). We next asked how Notch would affect the differentiation potential of pluripotent cells using this system. For that, we allowed sorted iChr-Notch-Mosaic ES cells to differentiate for 48 hours after LIF removal and analysed the expression of genes related to early differentiation at different time points (Fig 6C). On the one hand, we observed that the peak of expression of *Tle4*, and the early epiblast markers *Fgf5* and *Pou3f1* occurred earlier and remained at higher levels in Notch GOF than in wildtype ES cells. On the other hand, Notch LOF cells never reached normal levels of *Tbx3* or *Fgf5* during the differentiation process (Fig 6E). These results suggest that Notch is not only sufficient to drive expression of some differentiation markers such as *Tle4*, but also necessary to achieve proper levels of others such as *Tbx3*. However, modulation of Notch levels is

not enough to change expression of pluripotency markers once ES cells have started the differentiation process (Fig S7C). Overall, our results suggest that Notch is involved in coordinating exit from pluripotency and promoting cell differentiation in ES cells, mirroring its role in the early embryo.

Discussion

During the first three days of mouse embryonic development, cells lose their totipotent capacity as they form the first differentiated population, the trophectoderm (TE). In this study, we show that Notch signalling regulates the early expression of *Cdx2*, a key element in TE specification, and that this is later reinforced by the input of Hippo signalling through YAP and TEAD4. Hippo has been shown to act as a readout of cell polarity [8,59] and it activates *Cdx2* in cells that have established an apical domain. However, the initial triggering of *Cdx2* both in inner and outer cells [21,22] suggested that inputs other than Hippo would initially be acting because its expression could not be explained only by YAP/TEAD4 activity. In fact, previous reports have described that although in most *Tead4*$^{-/-}$ blastocysts CDX2 is not detected; earlier *Tead4*$^{-/-}$ morulae retain CDX2 expression [33]. In agreement with these observations, we found blastomeres in the morula that express CDX2 but do not have nuclear YAP. In this situation, expression of CDX2 is likely due to Notch activity as the CBF1-VENUS reporter, used as a proxy for activity of the pathway [31], is present in those cells. The analysis of *Rbpj* and *Notch1* mutants in early and late morulae, as well as pharmacological treatments of preimplantation embryos, further support the notion that the input provided by Notch is necessary for the early phases of *Cdx2* expression. These results, together with the fact that Notch overexpression cannot fully rescue the *Tead4* mutant phenotype, shows that Notch and Hippo have non-redundant but partially overlapping roles in early and late phases of *Cdx2* expression, respectively.

Furthermore, only double knockout morulae for *Rbpj* and *Tead4* completely lack CDX2, and all CDX2 positive cells have at least one of the two pathways active. These findings support a model whereby overlapping or complementary inputs from different signalling pathways may provide robustness in the system, buffering any disturbances and ensuring proper development [60]. In such a model, Notch and Hippo would ensure the correct specification and maintenance of the TE respectively [16].

The crosstalk between YAP and Notch has been studied in different cellular contexts [61]. YAP acts upstream of Notch in controlling epidermal stem cell fate or liver cell fate [62,63] while Notch is upstream of YAP in the corneal epithelium during chronic inflammation [64]. Also, YAP and Notch can cooperate to control the onset of oscillations in the segmentation clock [65] and they interact to promote the expression of *Jag1* in smooth muscle cells [66]. During TE establishment, YAP and Notch have also been shown to interact through SBNO1, and act synergistically to regulate *Cdx2* [28]. In this context, our results show that both pathways are acting in parallel since there is no correlation among YAP and CBF1-VENUS expression levels in single blastomeres in morula stage embryos. In addition, loss of the NOTCH1 receptor or RBPJ does not affect YAP/TEAD4 localisation and vice versa, *Tead4* knockout does not alter CBF-VENUS expression in the blastocyst. Nevertheless, several components of the Hippo pathway are downregulated in *Rbpj*$^{-/-}$ morulae, so we cannot rule out the possibility of cross-transcriptional regulation between the pathways.

The role of Notch signalling in the specification of cell fates during development has been widely studied [67]. Notch promotes heterogeneities and reinforces differences between neighbouring cells, explaining the segregation of cell fates in multiple processes and in different species [68]. The heterogeneous activity of CBF-VENUS in the 4-cell stage coincides with the loss of cell equivalence and emergence of differences among blastomeres. Other factors have been shown to be differentially expressed among blastomeres of the 4-cell mouse embryo [10,12], suggesting that this

is the moment when cells lose their homogeneous state to start desynchronizing and differentiating. Interestingly, *Prdm14*, one of these factors, and Notch show divergent patterns of expression during development. *Prdm14* is first expressed at the 2- and 4-cell stage, to be turned off and then re-expressed in the ICM of the blastocyst and later in the primordial germ cells [12,69]. In contrast, the Notch pathway, as revealed by the CBF-Venus reporter, begins to be active at the 4-cell stage, it is active in most of the cells of the morula, and is later restricted to the TE of the blastocyst. After implantation, Notch activity is detected throughout the epiblast [31]. It has been suggested that *Prdm14* expression coincides with conditions where groups of cells show an undetermined state, while Notch is activated when cells transition towards their next developmental phase. Our results suggest that Notch would be regulating these transitions by downregulating *Prdm14* expression. In line with the upregulation of *Prdm14* in embryos that lack Notch activity, we observed in the RNA-seq data from *Rbpj*$^{-/-}$ morulae a downregulation of Fgf receptors (*Fgfr1*, *2* and *3*) and DNA methyltransferases (*Dnmt3b*, *Dnmt1*), which are known to be repressed by PRDM14 [50,70]. It is also interesting to note that in our mosaic ES cell experiments, Notch levels correlate with those of *Prdm14* and *Dppa3*, but not with other pluripotency markers such as *Nanog* or *Esrrb*. Therefore, Notch is not simply turning off the general pluripotency network to promote differentiation, but acting on a subset of early naïve pluripotency markers.

Interplay between Notch and chromatin remodellers has been reported in several situations [71]. Expression changes in chromatin modifiers precede the action of transcription factors that consolidate lineage choices during preimplantation development [12]. Therefore, these alterations suggest that *Rbpj*$^{-/-}$ embryos do not established correct epigenetic landscapes, do not switch off early markers such as *Prdm14* or *Dppa3* and are not able to properly trigger differentiation programs leading to a delay in the expression of lineage specifiers such as *Cdx2*. In this regard, it is

interesting to note that *Rbpj* mutant morulae downregulate *Chaf1a*, which encodes the large subunit of the histone-chaperone CAF-1. Loss of CAF-1 promotes ES cells to transit to an earlier, totipotent 2-cell-like state [72], and acts as a barrier for reprogramming [73]. Furthermore, knockout of *Chaf1a* leads to developmental arrest at the 16-cell stage and a loss of heterochromatin [74]. Thus, CAF-1 acts as a driver of differentiation in pluripotent cells. Interestingly, studies in *Drosophila* have shown that CAF-1 mediates downstream effect of the Notch pathway [75]. On the other hand, *Asf1a*, which encodes another histone chaperone, is among the few genes observed to be upregulated in *Rbpj*$^{-/-}$ embryos. Forced expression of *Asf1a* promotes reprogramming of human ES cells [76], revealing a critical role in maintaining pluripotency. Furthermore, regulators of H3K9me3-heterochromatin that restrict cell plasticity and stemness, such as those encoded by *Setdb1* or *Suv39h1* [77], are also downregulated in Notch loss-of-function morulae. In conclusion, we observed that during preimplantation development, Notch regulates critical epigenetic components that mediate transitions along the progressive restriction of potency that occurs in the early embryo.

In this study, we have also identified novel putative targets positively regulated by the Notch pathway, such as *Tle4* and *Tbx3* whose role in the exit from pluripotency has been described in ES cells [53–55]. Their increase in expression from 2-cell to morula supports their possible role in promoting early differentiation *in vivo* as well. TLE4 does not bind directly to DNA, but associates with other proteins to act as a transcriptional corepressor [78]. It will be of great interest to identify its transcriptional partners during preimplantation development and elucidate the mechanism by which it allows cell differentiation in this context. The role of TBX3 is more complex since, in addition to promoting differentiation, it has also been associated with pluripotency maintenance [45,46]. Furthermore, *in vivo* TBX3 is detected in most of the cells of the morula but it is later restricted to the ICM [54], following a complementary pattern to Notch. Thus, *Tbx3*

regulation must involve Notch-dependant and Notch-independent inputs, what could explain why the mutation or deletion of the RBPJ motif present in the intronic *Tbx3* regulatory element did not disrupt enhancer activity or endogenous expression.

The role of Notch in ES cells had already been explored in the context of neural differentiation [79]. Blocking Notch signalling prevents ES cells from adopting a neural fate while its overexpression increases the frequency of neural specification. Our results suggest that Notch might have a more general role in promoting early differentiation, with a more specific function in neural specification at later stages [79]. In summary, our findings suggest that Notch acts by promoting the gradual loss of potency in the early embryo which is subsequently reinforced by additional mechanisms, such as heterochromatin formation before the morula stage, or differential activation of the Hippo pathway at the morula-to-blastocyst transition. Therefore, in order to correctly specify a given lineage, such as the trophectoderm, Notch is simultaneously activating fate choice markers such as *Cdx2* and inducing a differentiation-prone state by lowering levels of naïve markers.

Materials and Methods

Animal experimentation

The following mouse lines were used in this work: *CBF1-VENUS* [31], *Rbpj* null [80], *Tead4* null [33], *Notch1* null [81], *iChr-Notch-Mosaic* [40], *Rosa26-stop-N1ICD-ires-eGFP* [34], *Polr2a*^{CreERT2} [41], *Sox2*^{Cre} [35]. All the lines were maintained in heterozygosis in an outbred background. Adults were genotyped by PCR of tail-tip DNA using primers and conditions previously described for each line. For preimplantation embryos, genotyping was performed directly on individually isolated embryos after recovery, culture or antibody staining.

Mice were housed and maintained in the animal facility at the Centro Nacional de Investigaciones Cardiovasculares (Madrid, Spain) in accordance with national and European Legislation. Procedures were approved by the CNIC Animal Welfare Ethics Committee and by the Area of Animal Protection of the Regional Government of Madrid (ref. PROEX 196/14).

Embryo collection and culture

Females from the different mouse lines or outbred CD1 were superovulated as previously described [82], except in the case of embryos to be used for RNA-seq. For embryo culture, zygotes were collected from oviducts, treated with hyaluronidase (Sigma) to remove cumulus cells and cultured until the desired stage at 37.5°C, 5% CO_2, in M16 medium (Sigma) covered with mineral oil (NidOil, EVB). For experiments that did not require culture, embryos were collected at morula or blastocyst stage by flushing the oviduct or the uterus with M2 medium (Sigma) and fixed.

Immunofluorescence of preimplantation embryos

Immunofluorescence was performed as previously described (Dietrich and Hiiragi, 2007). The following antibodies and dilutions were used: monoclonal mouse anti-CDX2 (MU392-UC, BioGenex) 1:200, rabbit monoclonal anti-CDX2 (ab76541, Abcam) 1:200, mouse monoclonal anti-Oct4 (sc-5279, Santa Cruz Biotechnology) 1:200, mouse monoclonal anti-YAP (sc-101199, Santa Cruz Biotechnology) 1:200, rat monoclonal anti-NANOG (14-5761, eBioscience) 1:200, rabbit polyclonal anti-pERM (3141, Cell Signaling) 1:250, rat monoclonal anti-E-Cadherin (U3254, Sigma) 1:250, mouse monoclonal anti-TEAD4 (ab58310, Abcam) 1:100, rabbit polyclonal anti-DsRed (632496 living colors Clontech) 1:500, goat polyclonal anti-GFP (R1091P, Acris, Origene) 1:200, rat monoclonal anti-HA (11867423001, Sigma) 1:200. Secondary

Alexa Fluor conjugated antibodies (Life Technologies) were used at 1:1000. Nuclei were visualized by incubating embryos in DAPI at 1 µg/ml.

Imaging and quantification

Images of antibody-stained embryos were acquired on glass-bottomed dishes (Ibidi or MatTek) with a Leica SP5, Leica SP8 or Zeiss LSM880 laser scanning confocal microscopes. The same parameters were used for imaging each experiment. Semi-automated 3D nuclear segmentation for quantification of fluorescence intensity was carried out using MINS, a MATLAB-based algorithm (http://katlab-tools.org/) [32], and analysed as previously described [83]. Mitotic and pyknotic nuclei were excluded from the analysis.

For live imaging, embryos were cultured in microdrops of PBS on glass-bottomed dishes (MatTek) in an environmental chamber as described previously [84]. Images were acquired with a Zeiss LSM880 laser scanning confocal microscope system using a 40x objective. An optical section interval of 1.5 µm was acquired per z-stack, every 15 minutes.

Cell tracking of 3D-movies was carried out using a TrackMate plugin in Fiji [85–87]. The 3D reconstruction of the embryos and position of the cells was done using MatLab. The shape of the embryos was fitted into an ellipse and the coordinates in X, Y, Z for each blastomere were normalised to the centroid of the ellipse.

Pharmacological inhibitor treatments

Two-cell or morula stage embryos were cultured in drops of M16 medium (Sigma) covered with mineral oil (NidOil, EVB) at 37ºC, 5% CO_2, containing the corresponding pharmacological inhibitor or only DMSO as control until the corresponding stage. The

following inhibitors and concentrations were used: 10 or 20 μM of the γ-secretase inhibitor RO4929097 (S1575, Selleckchem) [36] and 10 μM of the TEAD/YAP inhibitor Verteporfin (Sigma) [37].

Quantitative-PCR

RNA from pools of 25-30 embryos (for pharmacological inhibitor experiments) or from single embryos (for CRISPR/Cas9 editing) was isolated using the Arcturus PicoPure RNA Isolation Kit (Applied Biosystems) and reverse transcribed using the Quantitect Kit (Qiagen). RNA was isolated from ES cells with the RNeasy Mini Kit (Qiagen) and reverse transcribed using the High Capacity cDNA Reverse Transcription Kit (Applied Biosystems). cDNA was used for quantitative-PCR (qPCR) with Power SYBR® Green (Applied Biosystems) in a 7900HT Fast Real-Time PCR System (Applied Biosystems). Expression of each gene was normalized to the expression of the housekeeping genes *Actin* (in mESC or pools of embryos) or *18S rRNA* (in single embryos). Primers used are detailed in Table S3.

RNA-sequencing data analysis

RNA-seq was performed on single morulae from the same litter. cDNA synthesis was performed using SMART-Seq Ultra Low Input RNA Kit (Clontech). Library preparation and sequencing was performed by the CNIC Genomics Unit using the Illumina HiSeq 2500 sequencer. Gene expression analysis was performed by the CNIC Bioinformatics Unit. Reads were mapped against the mouse transcriptome (GRCm38 assembly, Ensembl release 76) and quantified using RSEM v1.2.20 [88]. Raw expression counts were then processed with an analysis pipeline that used Bioconductor packages EdgeR [89] for normalisation (using TMM method) and differential expression testing. Expression data of *Rbpj* and *Neo* were used to genotype the samples. Two mutant and

three control (two wildtype and one heterozygote) embryos were selected for analysis. Changes in gene expression were considered significant if associated to Benjamini and Hochberg adjusted p-value < 0.05.

RBPJ binding motifs were located according to the consensus motif from CIS-BP database (M6499_1.02 motif) using FIMO [90]. Association of RBPJ motifs to DEG was performed using BEDTOOLS [91] using a 10 Kb window surrounding the transcriptional start site of genes. ATAC-seq data from 8-cell stage embryos [52] was mapped to the GRCm38 assembly and integrated with the coordinates of RBPJ motifs previously detailed.

Transient transgenic assay

For the generation of transient transgenics, F1 (C57Bl/6 x CBA) females were superovulated to obtain fertilized oocytes as described [82]. Each construct was microinjected into the pronucleus of fertilized oocytes at E0.5 at a concentration of 2 ng/µl. Microinjected oocytes were cultured in microdrops of M16 medium (Sigma) covered with mineral oil (NidOil, EMB) at 37°C, 5% CO_2 until the morula stage.

Each fragment to be tested was amplified from mouse genomic DNA and by means of NEBuilder HiFi DNA Assembly kit (New England Biolabs), they were cloned into a modified pBluescript vector [92] containing a H2BmRFP reporter gene under the control of the human beta-globin minimal promoter and including an SV40 polyadenylation signal. Primers for amplifying and cloning the 700 bp Tle4-up region are ctatagggcgaattggagctcTTCTTTAGAGGCACCAGTC and ggatccactagttctagagcggccgcATAAAGCCATTTTGCTTAACTG. Primers to amplify and clone the 600 bp Tbx3-i7 region are ctatagggcgaattggagctcCAAGCCAGCCTCAGTCCC and ggatccactagttctagagcggccgcCACACAAGCTTGCCAGCC. Lower case indicates

sequence annealing to the plasmid and capital letters indicates sequence annealing to the genome. Constructs were linearized and plasmid sequences removed before microinjection. For H2BmRFP detection, embryos were fixed in 4% paraformaldehyde for 10 min at room temperature and immunostained.

Mutagenesis

Mutated version of Tle4-up (Tle4-up mut^{RBPJ}) was generated by site-directed mutagenesis (Mutagenex Inc.), changing the TGTGGGAAA binding motif to TGTccGAAA. Mutated version of Tbx3-i7 (Tbx3-i7 mut^{RBPJ}) was generated using QuickChange II XL Site-Directed Mutagenesis Kit (Agilent Technologies) changing CGTGGGAAA to CGTccGAAA. Lower case indicates the altered residues. Changes that abolish RBPJ binding were based on previously described mutated versions of the binding site [93].

CRISPR/Cas9 genome editing

Two guide-RNAs at 60 ng/µl were incubated with tracRNA (Sigma) at 240 ng/µl for 5 min at 95ºC. The hybridised gRNAs were then incubated with the Cas9 protein (PNA bio) at 30 ng/µl for 15 min at RT and microinjected into the pronuclei of (CBAxC57) F1 zygotes. sgRNAs were designed using the CRISPOR tool (http://crispor.tefor.net/) [94]. The following guide RNAs were used: *Tle4*, TTAGCCTGCACTTCGAGTTA and CCCAATTCAAGGCGTTCTGT; *Tbx3*, TAACCCTTTAGAGATAGGCT and TACCAGAGAGGTTTCCTACT. Embryos were recovered at E2.5 and lysed in 50 µl extraction buffer from the Arcturus PicoPure RNA Isolation Kit (Applied Biosystems). Aliquots of 10 µl were used for DNA extraction for PCR genotyping. Mosaic embryos were those where we detected both the deleted and the wildtype allele. The remaining 40 µl were used for RNA extraction for RT-qPCR.

Cell culture

iChr-Notch-Mosaic ES cells were cultured in standard ESC media (DMEM, Gibco) supplemented with 15% foetal bovine serum (HyClone), 1% Glutamine, 1% NEAA (Hyclone), 0.1% ß-mercaptoethanol (Sigma) and LIF (produced in-house) in dishes seeded with a feeder layer of mouse embryonic fibroblasts (MEFs). Cells were transfected with a *Cre* expressing plasmid to induce recombination using Lipofectamine 2000 (Invitrogen) for 24 hours. After recombination, cells were sorted using a Becton Dickinson FACS Aria Cell Sorter. To promote spontaneous differentiation, cells were cultured on gelatine-covered dishes for 48 hours in DMEM (Gibco) supplemented with 20% serum, 1% Glutamine and 0.1% ß-mercaptoethanol (Sigma).

Statistics

Statistical analyses were performed with GraphPad Prism 7 or R studio. Data are presented as means ± s.d. or ± s.e.m. as indicated. Differences were considered statistically significant at p-value < 0.05. Tests used to calculate p-value are detailed in the figure legends. Student's t-test was used to compare two groups. ANOVA with Fisher or Bonferroni post-test was used to compare several groups. Fisher's exact test was used to compare distributions.

Acknowledgements

We thank Alba Álvarez for help with bioinformatics; Laura Fernandez de Manuel and Daniel Jimenez-Carretero for help with cell tracking; Jose Luis de la Pompa, Hiroshi Sasaki and Miguel Torres for mice lines; the CNIC Genomics, Microscopy and Bioinformatics Units for technical support; and members of Manzanares lab for

suggestions and discussions. This work was supported by the Spanish government (grants BFU2017-84914-P and BFU2015-72319-EXP to MM; FPI-SO Fellowship to SM); and grants NIH-R01DK084391, NIH-R01HD094868 and NIH-P30CA008748 to AKH. The CNIC is supported by the Spanish Ministry of Science, Innovation and Universities and the Pro CNIC Foundation, and is a Severo Ochoa Center of Excellence (SEV-2015-0505).

References

1. Wennekamp S, Mesecke S, Nédélec F, Hiiragi T. A self-organization framework for symmetry breaking in the mammalian embryo. Nat Rev Mol Cell Biol. 2013;14: 452–459. doi:10.1038/nrm3602

2. Cockburn K, Rossant J. Making the blastocyst: lessons from the mouse. J Clin Invest. 2010;120: 995–1003. doi:10.1172/JCI41229

3. Menchero S, Sainz de Aja J, Manzanares M. Our First Choice: Cellular and Genetic Underpinnings of Trophectoderm Identity and Differentiation in the Mammalian Embryo. Curr Top Dev Biol. 2018. pp. 59–80. doi:10.1016/bs.ctdb.2017.10.009

4. Sasaki H. Position- and polarity-dependent Hippo signaling regulates cell fates in preimplantation mouse embryos. Semin Cell Dev Biol. 2015;47–48: 80–87. doi:10.1016/J.SEMCDB.2015.05.003

5. Johnson MH, Ziomek CA. The foundation of two distinct cell lineages within the mouse morula. Cell. 1981;24: 71–80. doi:0092-8674(81)90502-X

6. Ziomek CA, Johnson MH. Cell surface interaction induces polarization of mouse 8-cell blastomeres at compaction. Cell. 1980;21: 935–942.

7. Tarkowski AK, Wroblewska J. Development of blastomeres of mouse eggs isolated at the 4- and 8-cell stage. J Embryol Exp Morphol. 1967;18: 155–180.

8. Anani S, Bhat S, Honma-Yamanaka N, Krawchuk D, Yamanaka Y. Initiation of Hippo signaling is linked to polarity rather than to cell position in the pre-implantation mouse embryo. Development. 2014;141: 2813–2824. doi:10.1242/dev.107276

9. Watanabe T, Biggins JS, Tannan NB, Srinivas S. Limited predictive value of blastomere angle of division in trophectoderm and inner cell mass specification.

Development. 2014;141: 2279–2288. doi:10.1242/dev.103267

10. Goolam M, Scialdone A, Graham SJ, Macaulay IC, Jedrusik A, Hupalowska A, et al. Heterogeneity in Oct4 and Sox2 Targets Biases Cell Fate in 4-Cell Mouse Embryos. Cell. 2016;165: 61–74. doi:10.1016/j.cell.2016.01.047

11. Torres-Padilla ME, Parfitt DE, Kouzarides T, Zernicka-Goetz M. Histone arginine methylation regulates pluripotency in the early mouse embryo. Nature. 2007;445: 214–218. doi:10.1038/nature05458

12. Burton A, Muller J, Tu S, Padilla-Longoria P, Guccione E, Torres-Padilla M-E. Single-Cell Profiling of Epigenetic Modifiers Identifies PRDM14 as an Inducer of Cell Fate in the Mammalian Embryo. Cell Rep. 2013;5: 687–701. doi:10.1016/j.celrep.2013.09.044

13. Chen Q, Shi J, Tao Y, Zernicka-Goetz M. Tracing the origin of heterogeneity and symmetry breaking in the early mammalian embryo. Nat Commun. 2018;9: 1819. doi:10.1038/s41467-018-04155-2

14. Maitre JL, Turlier H, Illukkumbura R, Eismann B, Niwayama R, Nedelec F, et al. Asymmetric division of contractile domains couples cell positioning and fate specification. Nature. 2016;536: 344–348. doi:10.1038/nature18958

15. Nishioka N, Inoue K, Adachi K, Kiyonari H, Ota M, Ralston A, et al. The Hippo signaling pathway components Lats and Yap pattern Tead4 activity to distinguish mouse trophectoderm from inner cell mass. Dev Cell. 2009;16: 398–410. doi:S1534-5807(09)00077-X

16. Rayon T, Menchero S, Nieto A, Xenopoulos P, Crespo M, Cockburn K, et al. Notch and hippo converge on Cdx2 to specify the trophectoderm lineage in the mouse blastocyst. Dev Cell. 2014;30: 410–422. doi:10.1016/j.devcel.2014.06.019

17. Korotkevich E, Niwayama R, Courtois A, Friese S, Berger N, Buchholz F, et al.

The Apical Domain Is Required and Sufficient for the First Lineage Segregation in the Mouse Embryo. Dev Cell. 2017;40: 235–247.e7. doi:10.1016/j.devcel.2017.01.006

18. Kono K, Tamashiro DAA, Alarcon VB. Inhibition of RHO-ROCK signaling enhances ICM and suppresses TE characteristics through activation of Hippo signaling in the mouse blastocyst. Dev Biol. 2014;394: 142–55. doi:10.1016/j.ydbio.2014.06.023

19. Mihajlovic AI, Bruce AW. Rho-associated protein kinase regulates subcellular localisation of Angiomotin and Hippo-signalling during preimplantation mouse embryo development. Reprod Biomed Online. 2016; doi:10.1016/j.rbmo.2016.06.028

20. Nissen SB, Perera M, Gonzalez JM, Morgani SM, Jensen MH, Sneppen K, et al. Four simple rules that are sufficient to generate the mammalian blastocyst. PLoS Biol. 2017;15: e2000737. doi:10.1371/journal.pbio.2000737

21. Dietrich JE, Hiiragi T. Stochastic patterning in the mouse pre-implantation embryo. Development. 2007;134: 4219–4231. doi:dev.003798

22. Posfai E, Petropoulos S, de Barros FR, Schell JP, Jurisica I, Sandberg R, et al. Position- and Hippo signaling-dependent plasticity during lineage segregation in the early mouse embryo. 2017;6. doi:10.7554/eLife.22906

23. Hirate Y, Hirahara S, Inoue K-I, Suzuki A, Alarcon VB, Akimoto K, et al. Polarity-dependent distribution of angiomotin localizes Hippo signaling in preimplantation embryos. Curr Biol. 2013;23: 1181–1194. doi:10.1016/j.cub.2013.05.014

24. Leung CY, Zernicka-Goetz M. Angiomotin prevents pluripotent lineage differentiation in mouse embryos via Hippo pathway-dependent and -independent mechanisms. Nat Commun. 2013;4: 2251. doi:10.1038/ncomms3251

25. Cockburn K, Biechele S, Garner J, Rossant J. The Hippo pathway member Nf2 is

required for inner cell mass specification. Curr Biol. 2013/06/25. 2013;23: 1195–1201. doi:10.1016/j.cub.2013.05.044

26. Wicklow E, Blij S, Frum T, Hirate Y, Lang RA, Sasaki H, et al. HIPPO pathway members restrict SOX2 to the inner cell mass where it promotes ICM fates in the mouse blastocyst. PLoS Genet. 2014;10: e1004618. doi:10.1371/journal.pgen.1004618

27. Ralston A, Cox BJ, Nishioka N, Sasaki H, Chea E, Rugg-Gunn P, et al. Gata3 regulates trophoblast development downstream of Tead4 and in parallel to Cdx2. Development. 2010;137: 395–403. doi:137/3/395

28. Watanabe Y, Miyasaka KY, Kubo A, Kida YS, Nakagawa O, Hirate Y, et al. Notch and Hippo signaling converge on Strawberry Notch 1 (Sbno1) to synergistically activate Cdx2 during specification of the trophectoderm. Sci Rep. 2017;7: 46135. doi:10.1038/srep46135

29. Ralston A, Rossant J. Cdx2 acts downstream of cell polarization to cell-autonomously promote trophectoderm fate in the early mouse embryo. Dev Biol. 2008;313: 614–29. doi:10.1016/j.ydbio.2007.10.054

30. Wu G, Gentile L, Fuchikami T, Sutter J, Psathaki K, Esteves TC, et al. Initiation of trophectoderm lineage specification in mouse embryos is independent of Cdx2. Development. 2010;137: 4159–69. doi:10.1242/dev.056630

31. Nowotschin S, Xenopoulos P, Schrode N, Hadjantonakis AK. A bright single-cell resolution live imaging reporter of Notch signaling in the mouse. BMC Dev Biol. 2013;13: 15. doi:1471-213X-13-15 [pii]10.1186/1471-213X-13-15

32. Lou X, Kang M, Xenopoulos P, Muñoz-Descalzo S, Hadjantonakis A-K. A Rapid and Efficient 2D/3D Nuclear Segmentation Method for Analysis of Early Mouse Embryo and Stem Cell Image Data. Stem Cell Reports. 2014;2: 382–397.

doi:10.1016/j.stemcr.2014.01.010

33. Nishioka N, Yamamoto S, Kiyonari H, Sato H, Sawada A, Ota M, et al. Tead4 is required for specification of trophectoderm in pre-implantation mouse embryos. Mech Dev. 2008;125: 270–283. doi:S0925-4773(07)00197-9

34. Murtaugh LC, Stanger BZ, Kwan KM, Melton DA. Notch signaling controls multiple steps of pancreatic differentiation. Proc Natl Acad Sci U S A. 2003;100: 14920–5. doi:10.1073/pnas.2436557100

35. Hayashi S, Tenzen T, McMahon AP. Maternal inheritance of Cre activity in a Sox2Cre deleter strain. Genesis. 2003;37: 51–3. doi:10.1002/gene.10225

36. Munch J, Gonzalez-Rajal A, de la Pompa JL. Notch regulates blastema proliferation and prevents differentiation during adult zebrafish fin regeneration. Development. 2013;140: 1402–1411. doi:10.1242/dev.087346

37. Liu-Chittenden Y, Huang B, Shim JS, Chen Q, Lee S-J, Anders RA, et al. Genetic and pharmacological disruption of the TEAD-YAP complex suppresses the oncogenic activity of YAP. Genes Dev. 2012;26: 1300–1305. doi:10.1101/gad.192856.112

38. McDole K, Zheng Y. Generation and live imaging of an endogenous Cdx2 reporter mouse line. Genesis. 2012;50: 775–782. doi:10.1002/dvg.22049

39. Toyooka Y, Oka S, Fujimori T. Early preimplantation cells expressing Cdx2 exhibit plasticity of specification to TE and ICM lineages through positional changes. Dev Biol. 2016;411: 50–60. doi:10.1016/j.ydbio.2016.01.011

40. Pontes-Quero S, Heredia L, Casquero-García V, Fernández-Chacón M, Luo W, Hermoso A, et al. Dual ifgMosaic: A Versatile Method for Multispectral and Combinatorial Mosaic Gene-Function Analysis. Cell. 2017;170: 800–814.e18. doi:10.1016/j.cell.2017.07.031

41. Guerra C, Mijimolle N, Dhawahir A, Dubus P, Barradas M, Serrano M, et al. Tumor induction by an endogenous K-ras oncogene is highly dependent on cellular context. Cancer Cell. 2003;4: 111–20.

42. Home P, Ray S, Dutta D, Bronshteyn I, Larson M, Paul S. GATA3 is selectively expressed in the trophectoderm of peri-implantation embryo and directly regulates Cdx2 gene expression. J Biol Chem. 2009;284: 28729–28737. doi:M109.016840

43. Home P, Kumar RP, Ganguly A, Saha B, Milano-Foster J, Bhattacharya B, et al. Genetic redundancy of GATA factors in the extraembryonic trophoblast lineage ensures the progression of preimplantation and postimplantation mammalian development. Development. 2017;144: 876–888. doi:10.1242/dev.145318

44. Haffner-Krausz R, Gorivodsky M, Chen Y, Lonai P. Expression of Fgfr2 in the early mouse embryo indicates its involvement in preimplantation development. Mech Dev. 1999;85: 167–172.

45. Han J, Yuan P, Yang H, Zhang J, Soh BS, Li P, et al. Tbx3 improves the germ-line competency of induced pluripotent stem cells. Nature. 2010;463: 1096–1100. doi:10.1038/nature08735

46. Niwa H, Ogawa K, Shimosato D, Adachi K. A parallel circuit of LIF signalling pathways maintains pluripotency of mouse ES cells. Nature. 2009;460: 118–122. doi:10.1038/nature08113

47. Yang J, Gao C, Chai L, Ma Y. A Novel SALL4/OCT4 Transcriptional Feedback Network for Pluripotency of Embryonic Stem Cells. PLoS One. 2010;5: e10766. doi:10.1371/journal.pone.0010766

48. Karantzali E, Lekakis V, Ioannou M, Hadjimichael C, Papamatheakis J, Kretsovali A. Sall1 Regulates Embryonic Stem Cell Differentiation in Association with Nanog. J Biol Chem. 2011;286: 1037–1045. doi:10.1074/jbc.M110.170050

49. Hayashi K, Lopes SMC de S, Tang F, Surani MA, Surani MA. Dynamic Equilibrium and Heterogeneity of Mouse Pluripotent Stem Cells with Distinct Functional and Epigenetic States. Cell Stem Cell. 2008;3: 391–401. doi:10.1016/j.stem.2008.07.027

50. Yamaji M, Ueda J, Hayashi K, Ohta H, Yabuta Y, Kurimoto K, et al. PRDM14 Ensures Naive Pluripotency through Dual Regulation of Signaling and Epigenetic Pathways in Mouse Embryonic Stem Cells. Cell Stem Cell. 2013;12: 368–382. doi:10.1016/J.STEM.2012.12.012

51. Burton A, Torres-Padilla M-E. Chromatin dynamics in the regulation of cell fate allocation during early embryogenesis. Nat Rev Mol Cell Biol. 2014;15: 723–735. doi:10.1038/nrm3885

52. Wu J, Huang B, Chen H, Yin Q, Liu Y, Xiang Y, et al. The landscape of accessible chromatin in mammalian preimplantation embryos. Nature. 2016;534: 652–657. doi:10.1038/nature18606

53. Laing AF, Lowell S, Brickman JM. Gro/TLE enables embryonic stem cell differentiation by repressing pluripotent gene expression. Dev Biol. 2015;397: 56–66. doi:10.1016/j.ydbio.2014.10.007

54. Russell R, Ilg M, Lin Q, Wu G, Lechel A, Bergmann W, et al. A Dynamic Role of TBX3 in the Pluripotency Circuitry. Stem Cell Reports. 2015;5: 1155–1170. doi:10.1016/j.stemcr.2015.11.003

55. Waghray A, Saiz N, Jayaprakash AD, Freire AG, Papatsenko D, Pereira C-F, et al. Tbx3 Controls Dppa3 Levels and Exit from Pluripotency toward Mesoderm. Stem cell reports. 2015;5: 97–110. doi:10.1016/j.stemcr.2015.05.009

56. Ran FA, Hsu PD, Wright J, Agarwala V, Scott DA, Zhang F. Genome engineering using the CRISPR-Cas9 system. Nat Protoc. 2013;8: 2281–2308.

doi:10.1038/nprot.2013.143

57. Kalkan T, Smith A. Mapping the route from naive pluripotency to lineage specification. Philos Trans R Soc B Biol Sci. 2014;369: 20130540–20130540. doi:10.1098/rstb.2013.0540

58. Hackett JA, Surani MA. Regulatory Principles of Pluripotency: From the Ground State Up. Cell Stem Cell. Cell Press; 2014;15: 416–430. doi:10.1016/J.STEM.2014.09.015

59. Hirate Y, Hirahara S, Inoue K, Kiyonari H, Niwa H, Sasaki H. Par-aPKC-dependent and -independent mechanisms cooperatively control cell polarity, Hippo signaling, and cell positioning in 16-cell stage mouse embryos. Dev Growth Differ. 2015;57: 544–556. doi:10.1111/dgd.12235

60. Menchero S, Rayon T, Andreu MJ, Manzanares M. Signaling pathways in mammalian preimplantation development: Linking cellular phenotypes to lineage decisions. Dev Dyn. 2017;246. doi:10.1002/dvdy.24471

61. Totaro A, Castellan M, Di Biagio D, Piccolo S. Crosstalk between YAP/TAZ and Notch Signaling. Trends Cell Biol. 2018;28: 560–573. doi:10.1016/j.tcb.2018.03.001

62. Yimlamai D, Christodoulou C, Galli GG, Yanger K, Pepe-Mooney B, Gurung B, et al. Hippo pathway activity influences liver cell fate. Cell. 2014;157: 1324–38. doi:10.1016/j.cell.2014.03.060

63. Totaro A, Castellan M, Battilana G, Zanconato F, Azzolin L, Giulitti S, et al. YAP/TAZ link cell mechanics to Notch signalling to control epidermal stem cell fate. Nat Commun. 2017;8: 15206. doi:10.1038/ncomms15206

64. Nowell CS, Odermatt PD, Azzolin L, Hohnel S, Wagner EF, Fantner GE, et al. Chronic inflammation imposes aberrant cell fate in regenerating epithelia through

mechanotransduction. Nat Cell Biol. 2016;18: 168–180. doi:10.1038/ncb3290

65. Hubaud A, Regev I, Mahadevan L, Pourquié O. Excitable Dynamics and Yap-Dependent Mechanical Cues Drive the Segmentation Clock. Cell. 2017;171: 668–682.e11. doi:10.1016/J.CELL.2017.08.043

66. Manderfield LJ, Aghajanian H, Engleka KA, Lim LY, Liu F, Jain R, et al. Hippo signaling is required for Notch-dependent smooth muscle differentiation of neural crest. Development. 2015;142: 2962–71. doi:10.1242/dev.125807

67. Koch U, Lehal R, Radtke F. Stem cells living with a Notch. Development. 2013;140: 689–704. doi:10.1242/dev.080614

68. Artavanis-Tsakonas S, Rand MD, Lake RJ. Notch signaling: cell fate control and signal integration in development. Science. 1999;284: 770–6. doi:10.1126/SCIENCE.284.5415.770

69. Yamaji M, Seki Y, Kurimoto K, Yabuta Y, Yuasa M, Shigeta M, et al. Critical function of Prdm14 for the establishment of the germ cell lineage in mice. Nat Genet. 2008;40: 1016–1022. doi:10.1038/ng.186

70. Grabole N, Tischler J, Hackett JA, Kim S, Tang F, Leitch HG, et al. Prdm14 promotes germline fate and naive pluripotency by repressing FGF signalling and DNA methylation. EMBO Rep. 2013;14: 629–637. doi:10.1038/embor.2013.67

71. Schwanbeck R. The Role of Epigenetic Mechanisms in Notch Signaling During Development. J Cell Physiol. 2015;230: 969–981. doi:10.1002/jcp.24851

72. Ishiuchi T, Enriquez-Gasca R, Mizutani E, Bošković A, Ziegler-Birling C, Rodriguez-Terrones D, et al. Early embryonic-like cells are induced by downregulating replication-dependent chromatin assembly. Nat Struct Mol Biol. 2015;22: 662–71. doi:10.1038/nsmb.3066

73. Cheloufi S, Elling U, Hopfgartner B, Jung YL, Murn J, Ninova M, et al. The histone

chaperone CAF-1 safeguards somatic cell identity. Nature. 2015;528: 218–24. doi:10.1038/nature15749

74. Houlard M, Berlivet S, Probst A V, Quivy J-P, Héry P, Almouzni G, et al. CAF-1 is essential for heterochromatin organization in pluripotent embryonic cells. PLoS Genet. 2006;2: e181. doi:10.1371/journal.pgen.0020181

75. Yu Z, Wu H, Chen H, Wang R, Liang X, Liu J, et al. CAF-1 promotes Notch signaling through epigenetic control of target gene expression during Drosophila development. Development. 2013;140: 3635–44. doi:10.1242/dev.094599

76. Gonzalez-Muñoz E, Arboleda-Estudillo Y, Otu HH, Cibelli JB. Cell reprogramming. Histone chaperone ASF1A is required for maintenance of pluripotency and cellular reprogramming. Science. 2014;345: 822–5. doi:10.1126/science.1254745

77. Yadav T, Quivy J-P, Almouzni G. Chromatin plasticity: A versatile landscape that underlies cell fate and identity. Science. 2018;361: 1332–1336. doi:10.1126/science.aat8950

78. Kaul AK, Schuster EF, Jennings BH. Recent insights into Groucho co-repressor recruitment and function. Transcription. 2015;6: 7–11. doi:10.1080/21541264.2014.1000709

79. Lowell S, Benchoua A, Heavey B, Smith AG. Notch promotes neural lineage entry by pluripotent embryonic stem cells. PLoS Biol. 2006;4: e121. doi:10.1371/journal.pbio.0040121

80. Oka C, Nakano T, Wakeham A, de la Pompa JL, Mori C, Sakai T, et al. Disruption of the mouse RBP-J kappa gene results in early embryonic death. Development. 1995;121: 3291–301.

81. Conlon RA, Reaume AG, Rossant J. Notch1 is required for the coordinate segmentation of somites. Development. 1995;121: 1533–1545.

82. Behringer R, Gertsenstein M, Vintersten Nagy K, Nagy A. Manipulating the Mouse Embryo: A Laboratory Manual. Fourth. New York: John Inglis; 2014.

83. Saiz N, Kang M, Schrode N, Lou X, Hadjantonakis A-K. Quantitative Analysis of Protein Expression to Study Lineage Specification in Mouse Preimplantation Embryos. J Vis Exp. 2016; 53654. doi:10.3791/53654

84. Xenopoulos P, Kang M, Puliafito A, Di Talia S, Hadjantonakis A-K. Heterogeneities in Nanog Expression Drive Stable Commitment to Pluripotency in the Mouse Blastocyst. Cell Rep. 2015;10: 1508–1520. doi:10.1016/J.CELREP.2015.02.010

85. Tinevez J-Y, Perry N, Schindelin J, Hoopes GM, Reynolds GD, Laplantine E, et al. TrackMate: An open and extensible platform for single-particle tracking. Methods. 2017;115: 80–90. doi:10.1016/J.YMETH.2016.09.016

86. Schindelin J, Arganda-Carreras I, Frise E, Kaynig V, Longair M, Pietzsch T, et al. Fiji: an open-source platform for biological-image analysis. Nat Methods. 2012;9: 676–682. doi:10.1038/nmeth.2019

87. Fernández-de-Manúel L, Díaz-Díaz C, Jiménez-Carretero D, Torres M, Montoya MC. ESC-Track: A computer workflow for 4-D segmentation, tracking, lineage tracing and dynamic context analysis of ESCs. Biotechniques. 2017;62: 215–222. doi:10.2144/000114545

88. Li B, Dewey CN. RSEM: accurate transcript quantification from RNA-Seq data with or without a reference genome. BMC Bioinformatics. 2011;12: 323. doi:10.1186/1471-2105-12-323

89. Robinson MD, McCarthy DJ, Smyth GK. edgeR: a Bioconductor package for differential expression analysis of digital gene expression data. Bioinformatics. 2010;26: 139–40. doi:10.1093/bioinformatics/btp616

90. Grant CE, Bailey TL, Noble WS. FIMO: scanning for occurrences of a given motif.

Bioinformatics. 2011;27: 1017–1018. doi:10.1093/bioinformatics/btr064

91. Quinlan AR, Hall IM. BEDTools: a flexible suite of utilities for comparing genomic features. Bioinformatics. 2010;26: 841–842. doi:10.1093/bioinformatics/btq033

92. Yee SP, Rigby PW. The regulation of myogenin gene expression during the embryonic development of the mouse. Genes Dev. 1993;7: 1277–89.

93. Tun T, Hamaguchi Y, Matsunami N, Furukawa T, Honjo T, Kawaichi M. Recognition sequence of a highly conserved DNA binding protein RBP-J kappa. Nucleic Acids Res. 1994;22: 965–71.

94. Haeussler M, Schönig K, Eckert H, Eschstruth A, Mianné J, Renaud J-B, et al. Evaluation of off-target and on-target scoring algorithms and integration into the guide RNA selection tool CRISPOR. Genome Biol. 2016;17: 148. doi:10.1186/s13059-016-1012-2

Figure legends

Fig 1. CDX2 expression depends on Notch and Hippo inputs. (A) Maximal projections of confocal images after immunostaining for CDX2 and OCT4 in different combinations of wildtype and mutant alleles for *Rbpj* and *Tead4* at E2.5. Scale bars, 20 μm. (B) Optical sections of confocal images after immunostaining for CDX2 and YAP in the CBF1-VENUS reporter line at morula (upper row) and blastocyst (lower row) stage. Fluorescent VENUS reporter is directly detected. Arrowheads indicate a cell positive for CDX2 and VENUS, but negative for nuclear YAP. Nuclei were stained with DAPI. Scale bars, 20 μm. (C-D) Pairwise correlations of single cell fluorescence intensity levels for CDX2, VENUS and YAP from embryos represented at morula (C) and blastocyst (D) stage. Person correlation (R^2) is indicated for each correlation. (E-F) Three-way correlations of single cell fluorescence intensity levels for CDX2, VENUS and YAP from embryos represented at morula (E) and blastocyst (F) stage. Cronbach Alpha (α) to measure internal consistency reliability among the three variables is indicated. (G) Venn diagram showing number of positive cells for CBF1-VENUS, YAP and CDX2 at morula stage. n=415 blastomeres from 28 embryos (morula stage); n=428 blastomeres from 6 embryos (blastocysts).

Fig 2. Notch regulates CDX2 in the early morula. (A-B) Relative expression of *Cdx2*, *Gata3*, *Oct4* and *Nanog* in pools of 25 embryos treated with RO4929097 to inhibit Notch (left) or Verteporfin to inhibit YAP/TEAD interaction (right), from the 2-cell to morula stage (A; n=6) or from morula to blastocyst stage (B; Notch inhibition, n=4-6; Hippo inhibition, n=6-11). Pools of embryos treated with DMSO were used as controls. * p-value < 0.05 by Student's t test. (C) Optical sections of confocal images after immunostaining of CDX2 in wildtype and *Rbpj*$^{-/-}$ early morulae. (D) Quantification of number of CDX2 positive cells in early morulae (n=11 embryos). (E) Optical sections of

confocal images after immunostaining of CDX2 in wildtype and *Rbpj*$^{-/-}$ late morulae. (F) Quantification of number of CDX2 positive cells in late morulae (Wildtype, n=4 embryos; *Rbpj*$^{-/-}$, n=5 embryos). Nuclei were stained with DAPI. Scale bar, 20 μm. Data are means ± s.d. *** p<0.001 by Fisher's exact test.

Fig 3. CBF1-VENUS dynamics in the mouse preimplantation embryo. (A) Maximal projections of confocal images of CBF1-VENUS reporter line in 4-cell, 6-cell, 8-cell and compacted morula stages. Immunostaining of pERM (bottom row) confirms acquisition of apical polarity in compacted morulae. Nuclei were stained with DAPI. Scale bar, 20 μm. (B) Percentage of VENUS positive cells per embryo at different stages (4-5 cell embryos, n=24; 6-7 cell embryos, n=7; 8-cell embryos, n=9). (C) Maximal projections of four time-frames during live imaging of embryos from the CBF1-VENUS reporter line. Time since the onset of time lapse is indicated. (D) 3D reconstruction of the time-lapse imaging of a representative embryo. A selected cell and its progeny are highlighted in orange. Blue blastomeres indicate inner position and grey blastomeres indicate outer position. (E) Mean intensity levels of VENUS in all the families of the live imaged embryos (n=7) according to the position of a cell and their progeny in the first and the final time frame. (F) Initial intensity levels of VENUS in all the families of the live imaged embryos according to the position of a cell and their progeny in the first and the final time frame. For (E) and (F), n=13 families for IN-ICM, n=11 families for IN–TE+ICM, n=55 families for OUT TE, n=16 families for OUT–TE+ICM. *** p<0.001, * p<0.05 by ANOVA with Bonferroni post-test.

Fig 4. Differences in Notch activity drive cell fate in the preimplantation embryo. (A) Schematic diagram of the experimental strategy, where iChr-Notch-Mosaic mice were crossed with Polr2a^{CreERT2} driver. Embryos were collected and treated with 4OH-

Tamoxifen from 2- to 4-cell stage to induce recombination. At morula and blastocyst stage, embryos were fixed and immunostained. (B) Optical section of confocal images after immunostaining for RFP, GFP and HA. Arrowheads indicate examples of cells recombined for the wildtype cassette (red), the Notch loss of function cassette (LOF, green) or the Notch gain of function cassette (GOF, blue). Nuclei were stained with DAPI. Scale bars, 20 μm. (C) Percentage of cells recombined for each cassette (n=11). (D-E) Percentage of cells for each cassette that are in are inner or outer position at the morula (D; wildtype, n=21; LOF, n=6; GOF, n=44) or blastocyst stage (E; wildtype, n=75; LOF, n=26; GOF, n=131). ** p<0.01, **** p<0.0001 by Fisher's exact test.

Fig 5. *Tle4* is a direct transcriptional target of Notch. (A) Volcano plot of differentially expressed genes between wildtype and *Rbpj*$^{-/-}$ single morulae. In blue, genes downregulated in *Rbpj*$^{-/-}$ (p-adj<0.05 and logFC < -1); in orange, genes upregulated in *Rbpj*$^{-/-}$ (p-adj<0.05 and logFC > 1). Representative genes are indicated. (B) Number of differentially expressed genes (DEG) between wildtype and *Rbpj*$^{-/-}$ morulae (top), those that have a RBPJ motif in a 10 Kb window surrounding the gene (middle), and those in which this site is included in an open chromatin ATAC-seq peak in 8-cell embryos [52] (bottom). (C) *Tbx3* and *Tle4* relative expression in pools of 25 embryos after treatment with RO4929097 to block Notch from 2-cell to morula stage. Pools of embryos treated with DMSO were used as controls. (D) Genomic landscape of the region upstream *Tle4* indicating the location of the RBPJ motif and the ATAC-seq track. (E) Maximal projection confocal images after RFP immunostaining of representative transgenic embryos for the region highlighted in pink in (D) (top) or the mutated version for the RBPJ site (bottom). Nuclei were stained with DAPI. Scale bar, 20 μm. (F) Percentage of positive embryos in the transient transgenic assay of Tle4-up region (n=137) or the mutated version (n=169). (G) *Tle4* relative expression in single embryos (wildtype, n=14; mosaic, n=9; deleted, n=10) after CRISPR/Cas9 deletion of

the region containing the RBPJ motif. Data are means ± s.d. * p<0.05 by Student's t test in (C) and (G). ** p<0.01 by Student's t test in (G) or by Fisher's exact test in (F).

Fig 6. Notch promotes exit from naïve pluripotency and cell differentiation of ES cells. (A) Construct showing the wildtype (red), Notch loss of function (green) and Notch gain of function (blue) cassettes from iChr-Notch-Mosaic ES cells. (B) Schematic diagram of experimental design, where iChr-Notch-Mosaic ES cells were recombined with Cre and sorted according to Notch activity. (C) *Prdm14*, *Dppa3*, *Nanog* and *Esrrb* relative expression in iChr-Notch-Mosaic ESCs after sorting of Notch LOF, Wildtype and Notch GOF populations (n=13 for *Prdm14*, n=17 for *Dppa3*, n=16 for *Nanog*, n=11 for *Esrrb*). (D) Schematic diagram of experimental design, where sorted recombined iChr-Notch-Mosaic ES cells were differentiated after LIF removal. (E) *Tle4*, *Tbx3*, *Fgf5* and *Pou3f1* relative expression in Notch LOF, Wildtype and Notch GOF cells at 0h, 12h, 24h and 48h after LIF withdrawal (n=6). Data are means ± s.e.m. * p<0.05, ** p<0.01, *** p<0.001, **** p<0.0001 by ANOVA with Fisher post-test.

Supplementary Figure legends

Fig S1. Lack of *Rbpj* and *Tead4* does not affect compaction or polarization. Single confocal plane for E-cadherin immunostaining (top row), and maximal projections of confocal images after immunostaining for E-Cadherin and pERM (middle row) in different combinations of wildtype and mutant alleles for *Rbpj* and *Tead4* at E2.5. Nuclei were stained with DAPI. Scale bars, 20 μm.

Fig S2. Notch and Hippo act independently in the blastocyst. (A-B) Maximal projections of confocal images after immunostaining for TEAD4 (A) or YAP (B) in wildtype and *Rbpj*$^{-/-}$ embryos. (C-D) Maximal projections of confocal images after immunostaining for TEAD4 (C) or YAP (D) in wildtype and *Notch1*$^{-/-}$ embryos. (E) Maximal projections of confocal images of the CBF1-VENUS line in wildtype and *Tead4*$^{-/-}$ embryos. (F) Maximal projections of confocal images after immunostaining for CDX2 and GFP in wildtype, *Tead4*$^{-/-}$, and N1ICD-GFP;*Tead4*$^{-/-}$ embryos. (G) Quantification of CDX2 intensity levels in *Tead4*$^{-/-}$ (n=75 blastomeres from 2 embryos) and N1ICD-GFP;*Tead4*$^{-/-}$ (n=224 blastomeres from 5 embryos) embryos. *** $p<0.001$ by Student's t-test.

Fig S3. Downregulation of CDX2 in *Notch1*$^{-/-}$ early morulae. (A) Optical sections of confocal images after immunostaining of CDX2 in wildtype and *Notch1*$^{-/-}$ early morulae. (B) Quantification of the number of CDX2 positive cells in wildtype (n=11) and *Notch1*$^{-/-}$ (n=11) early morulae. (C) Optical sections of confocal images after immunostaining of CDX2 in wildtype and *Notch1*$^{-/-}$ late morulae. (D) Quantification of the number of CDX2 positive cells in wildtype (n=5) and *Notch1*$^{-/-}$ (n=3) late morulae. Nuclei were stained with DAPI. Scale bars, 20 μm. *** $p<0.001$ by Fisher's exact test.

Fig S4. CBF1-VENUS activity during preimplantation development. (A) Percentage of VENUS positive cells in individual embryos of 4- to 8-cell stage (indicated on the x-axis) from the CBF1-VENUS line. (B) Cell tracking and family tree (each family in a different colour) after live imaging of a CBF1-VENUS embryo from morula to blastocyst stage (see Movie 1). (C) Percentage of cells from the ICM or from the TE according to the position (IN/OUT) of their progenitor cell in the first frame of the time lapse (n=7). (D-F) Representative examples of VENUS intensity levels of cells from families with different outcomes relating to their position in the first and final frame of the time lapse movies.

Fig S5. Confronting Notch activity levels in the preimplantation embryo. (A-B) Percentage of cells recombined for each cassette (wildtype, red; LOF, green; GOF, blue) in individual morulae (A) or blastocysts (B) from the iChr-Notch-Mosaic mouse line.

Fig S6. Transcriptome analysis of *Rbpj*$^{-/-}$ single morulae. (A) Hierarchical clustering separates control (wildtype and heterozygotes) from *Rbpj*$^{-/-}$ embryos. (B-C) log FC of selected differentially expressed genes between control and *Rbpj*$^{-/-}$ embryos related with lineage programs (B) or chromatin modifiers (C). (D) Genomic landscape of the region surrounding the seventh intron of *Tbx3* indicating the location of the RBPJ motif and the ATAC-seq track. (E) Maximal projection confocal images after RFP immunostaining of representative transgenic embryos for the region highlighted in pink in (D) (top) or the mutated version for the RBPJ site (bottom). Nuclei were stained with DAPI. Scale bars, 20 μm. (F) Percentage of positive embryos in the transient

transgenic assay of Tbx3-i7 region (n=75) or the mutated version (n=80). (G) *Tbx3* relative expression in single embryos (wildtype, n=7; mosaic, n=9; deleted, n=10) after CRISPR/Cas9 deletion of the region containing the RBPJ motif. Data are means ± s.d.

Fig S7. Expression of naïve pluripotency markers in the preimplantation embryo and in differentiating ES cells. (A) Expression of *Pdrm14*, *Dppa3*, *Tle4* and *Tbx3* in 2-cell, 4-cell and 8-cell stage single-cell RNA-seq data from Goolam [10]. (B) *Dppa3* and *Prdm14* relative expression in pools of 30 embryos after treatment with RO4929097 to block Notch from 2-cell to 4-cell stage. Pools of embryos treated with DMSO were used as controls. (C) *Nanog*, *Prdm14* and *Dppa3* relative expression in Notch LOF, Wildtype and Notch GOF ES cells at 0h, 12h, 24h and 48h after LIF withdrawal to promote differentiation (n=6). Data are means ± s.d. in (A) and (B) or ± s.e.m in (C). * $p<0.05$, ** $p<0.01$, *** $p<0.001$, **** $p<0.0001$ by ANOVA with Fisher post-test in (A) and (C) or by Student's t-test in (B).

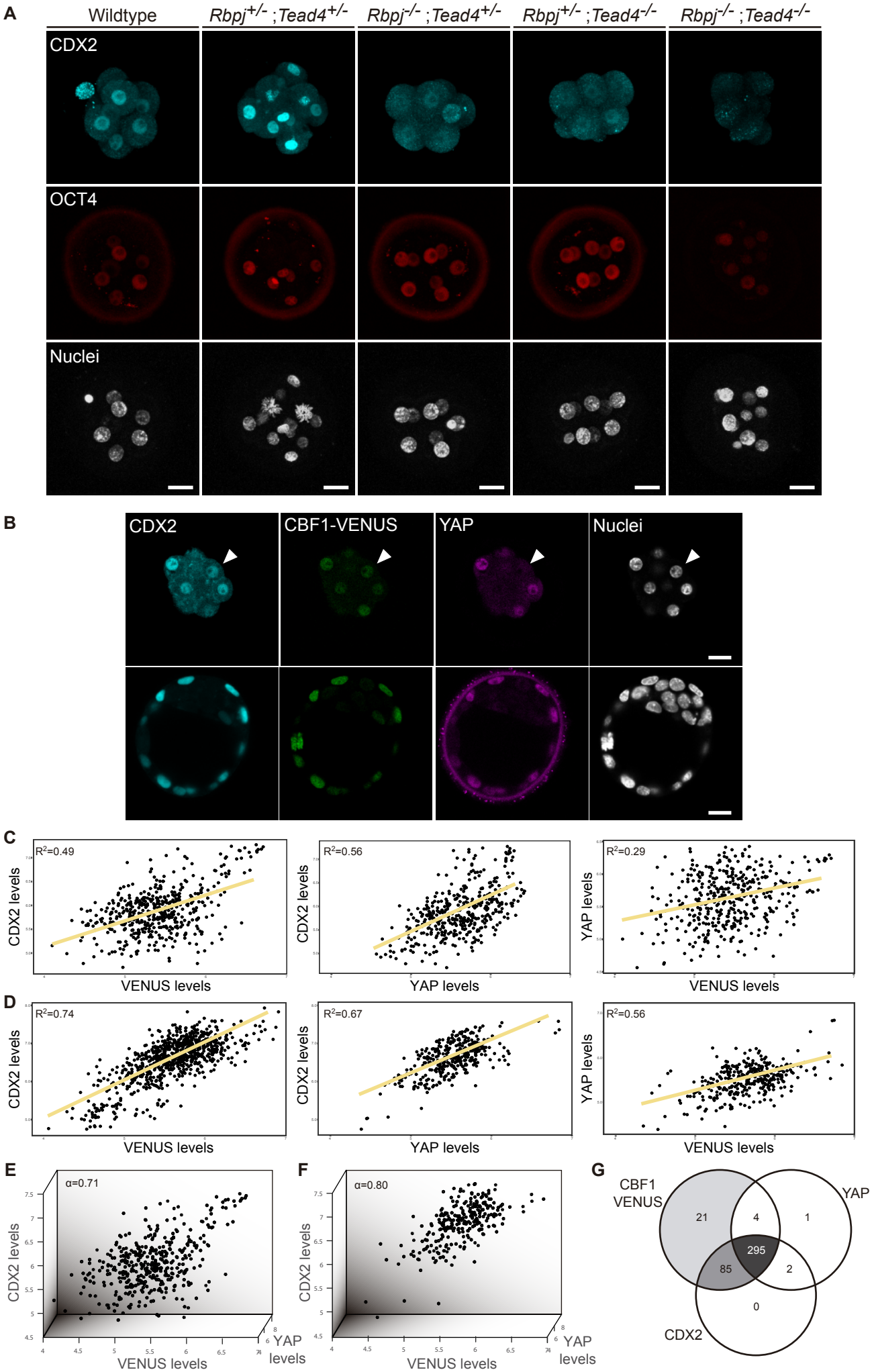

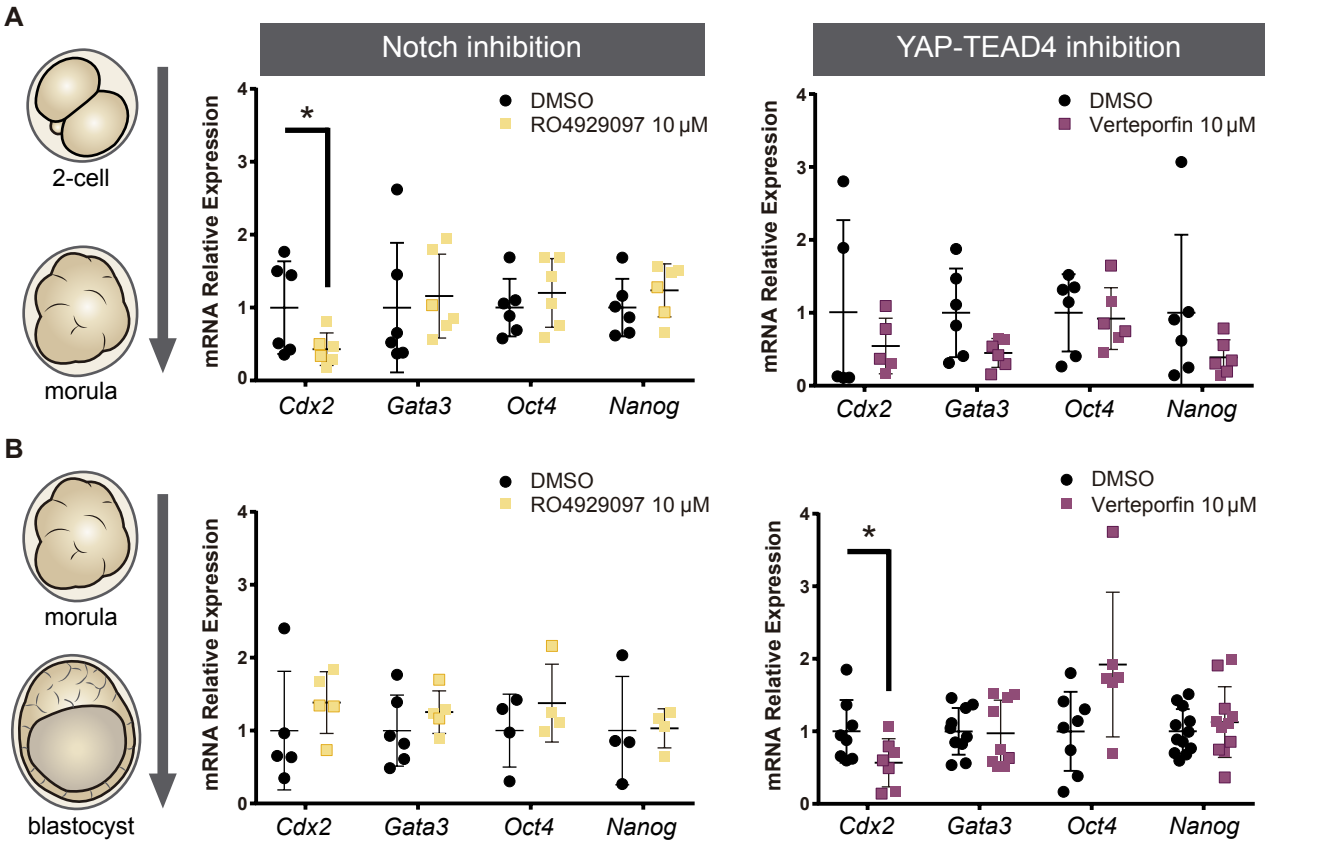

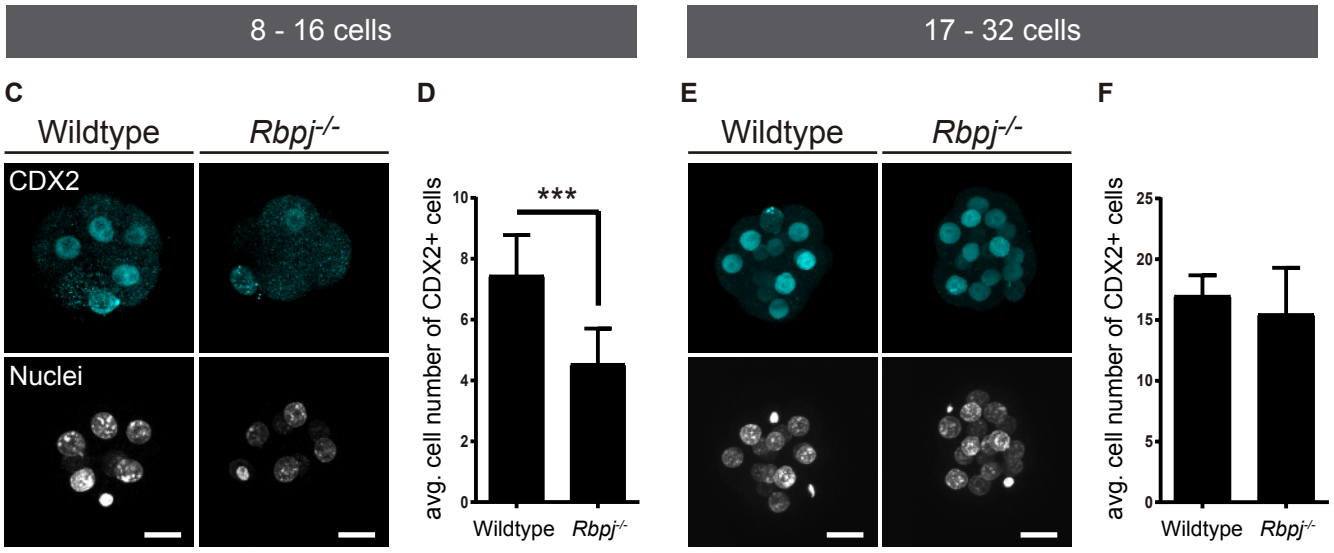

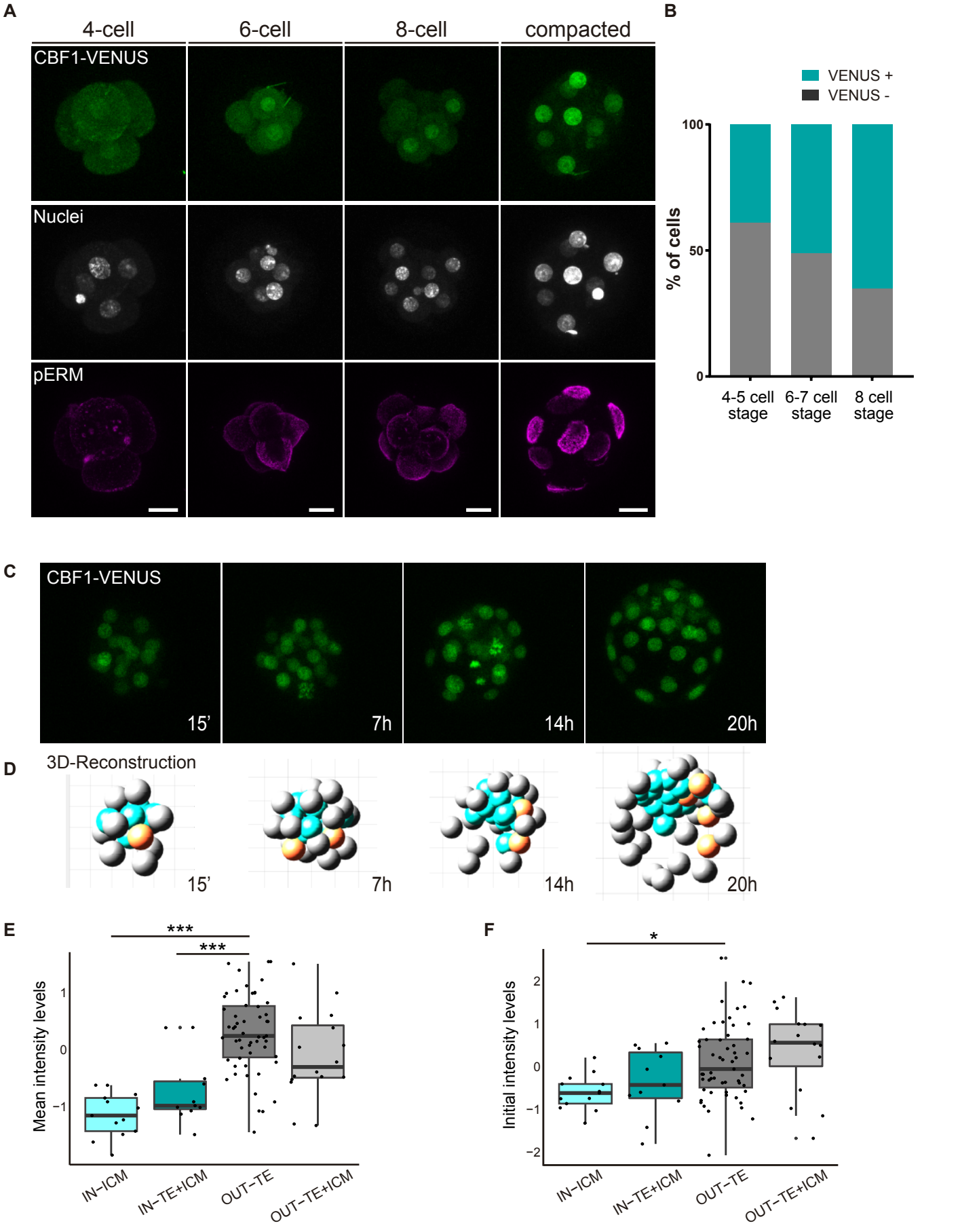

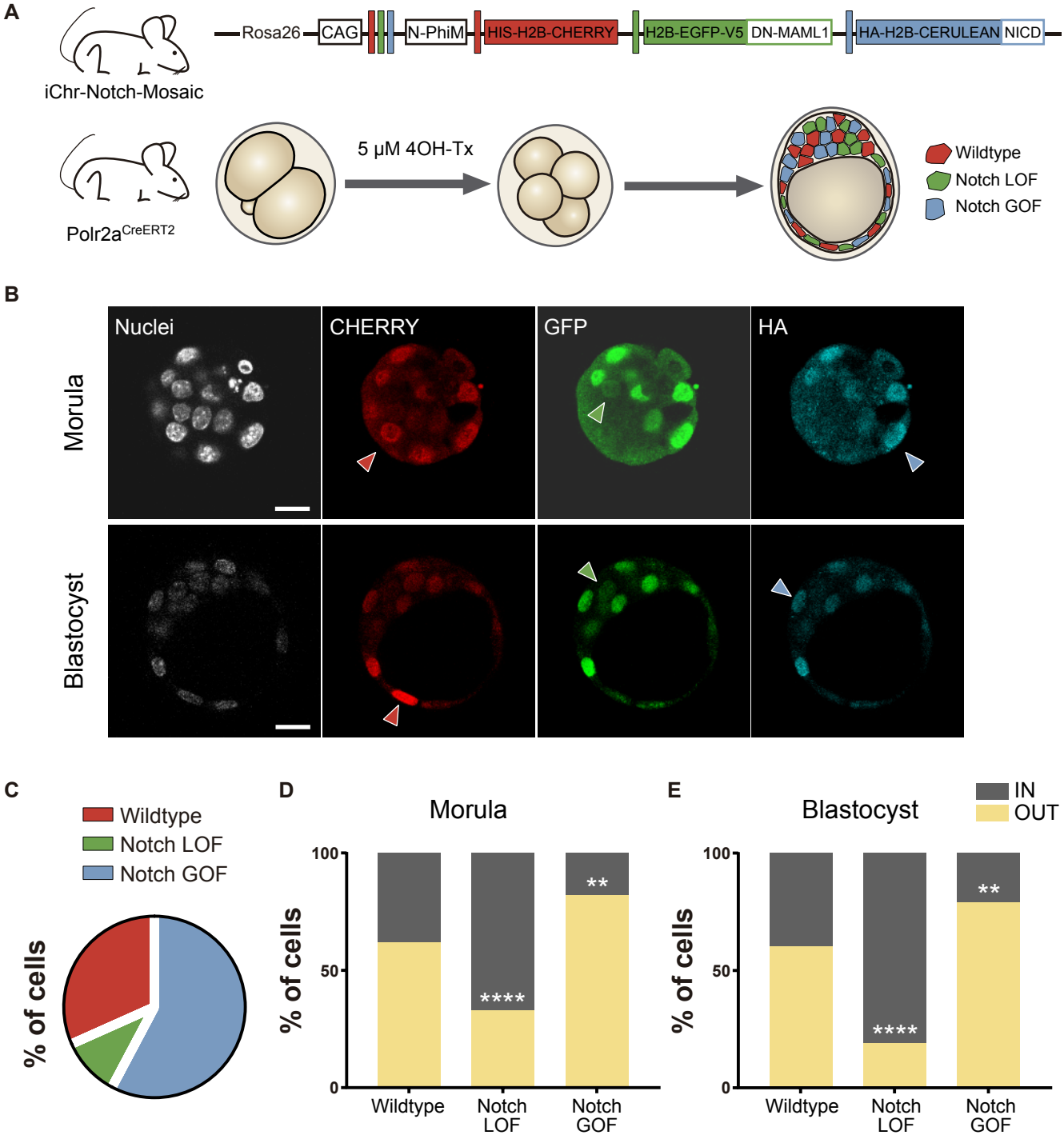

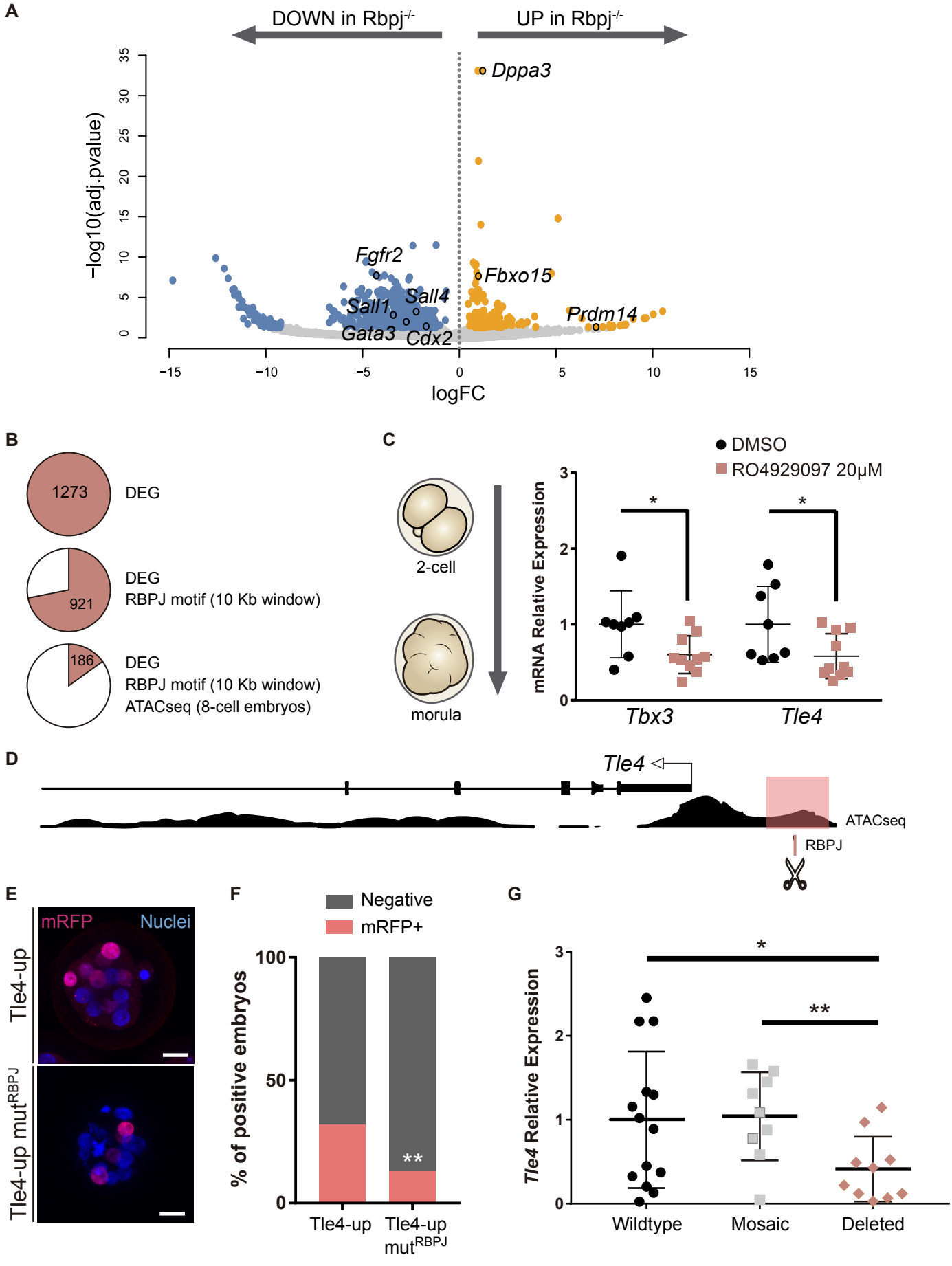

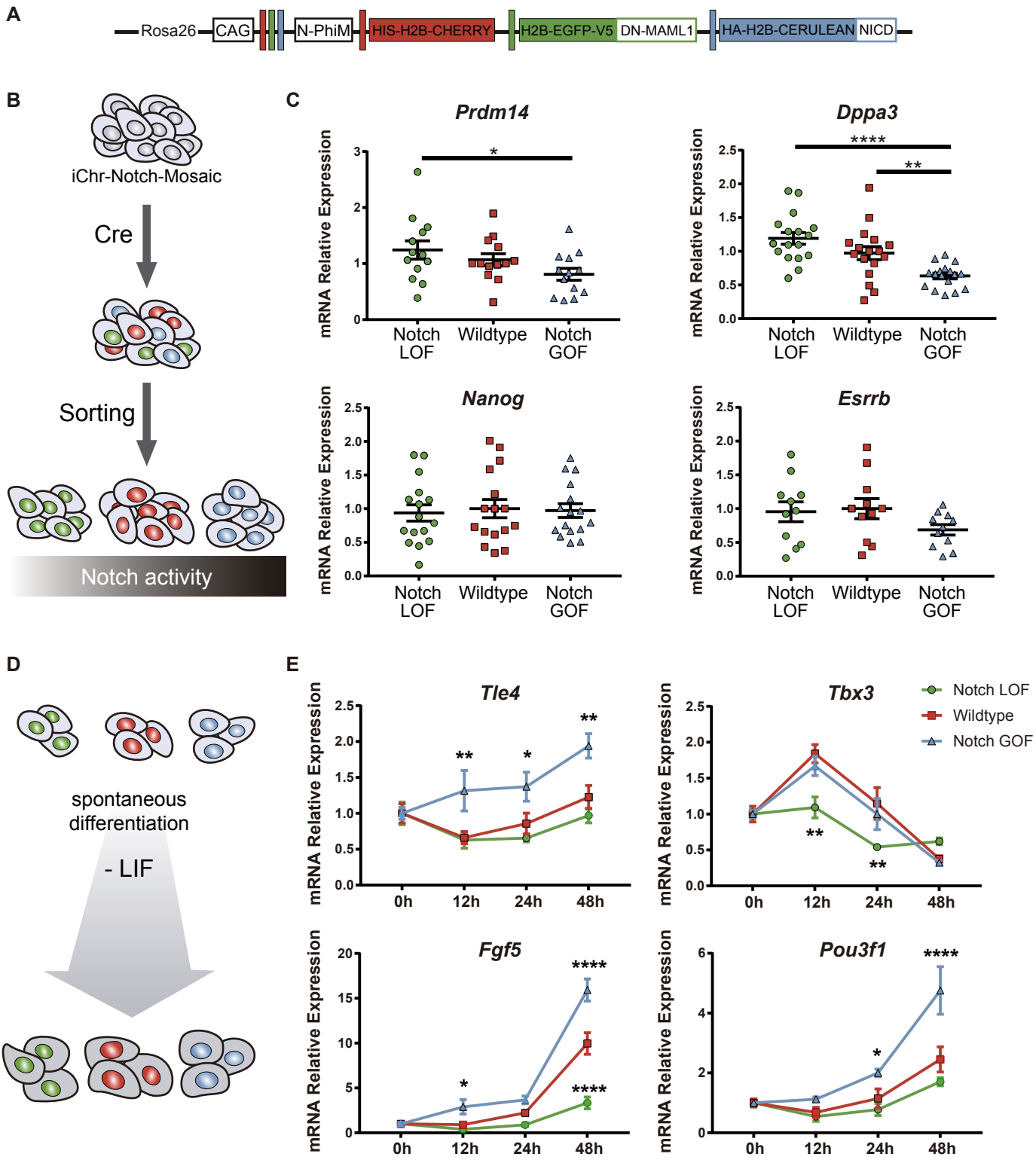

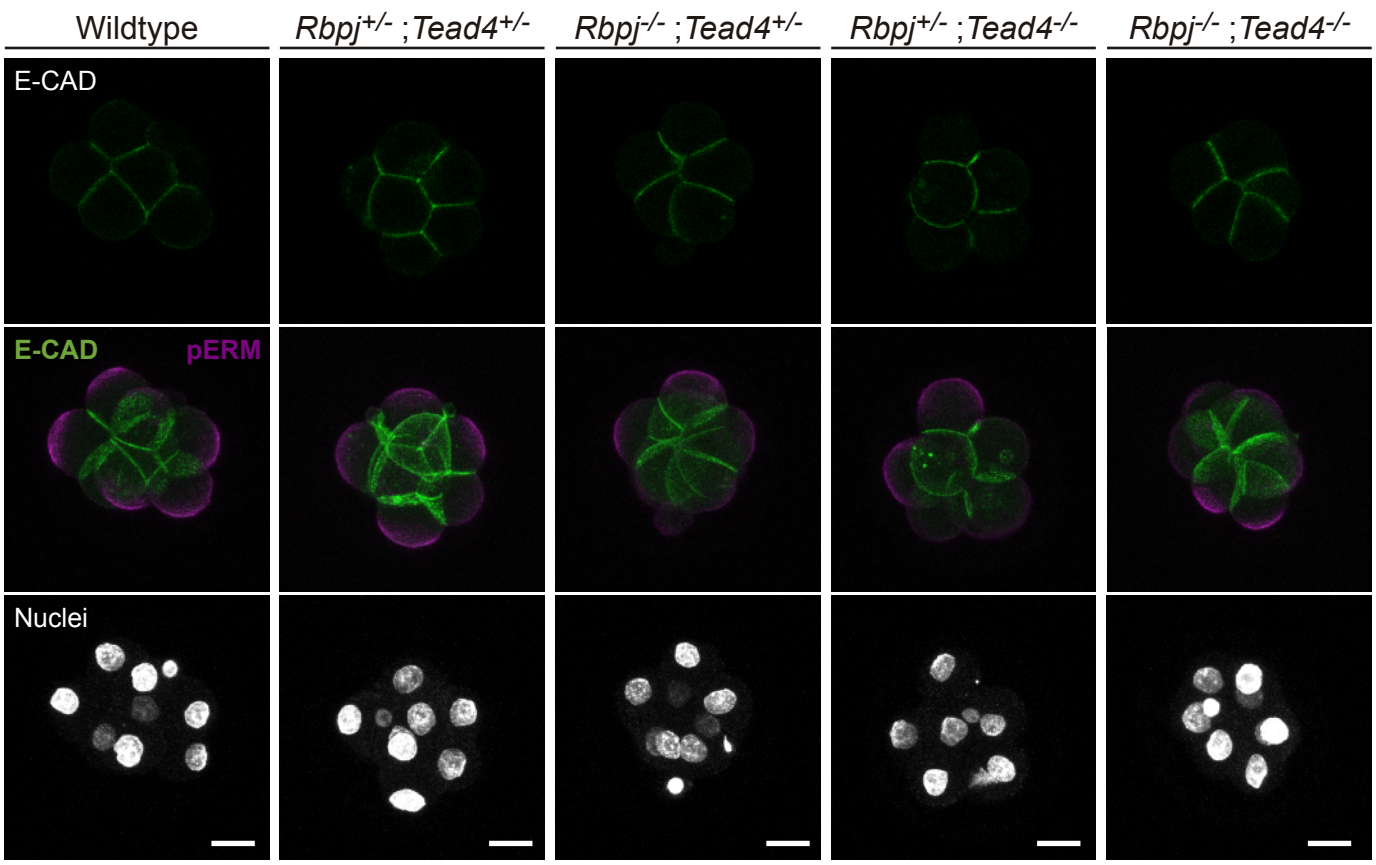

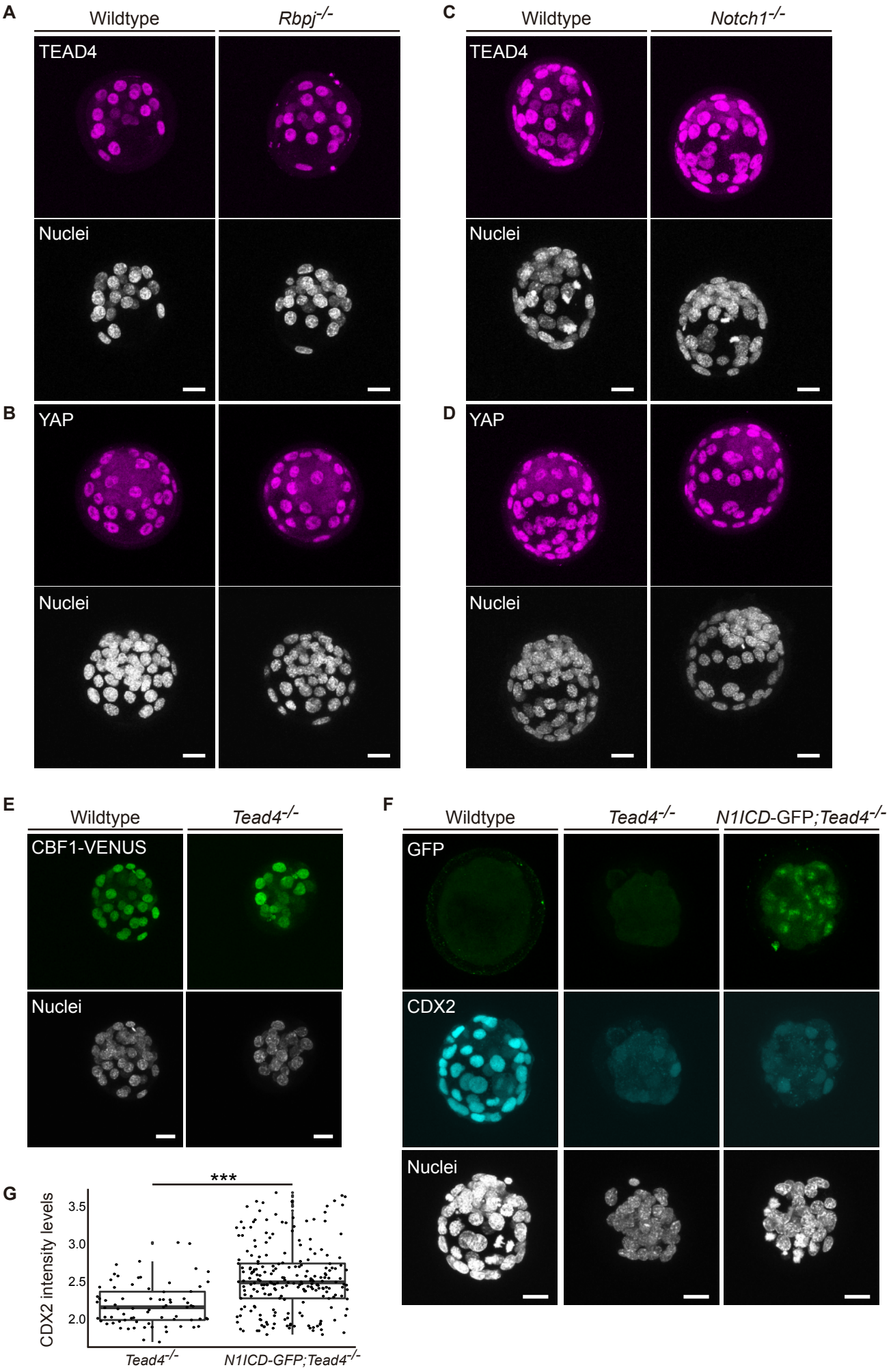

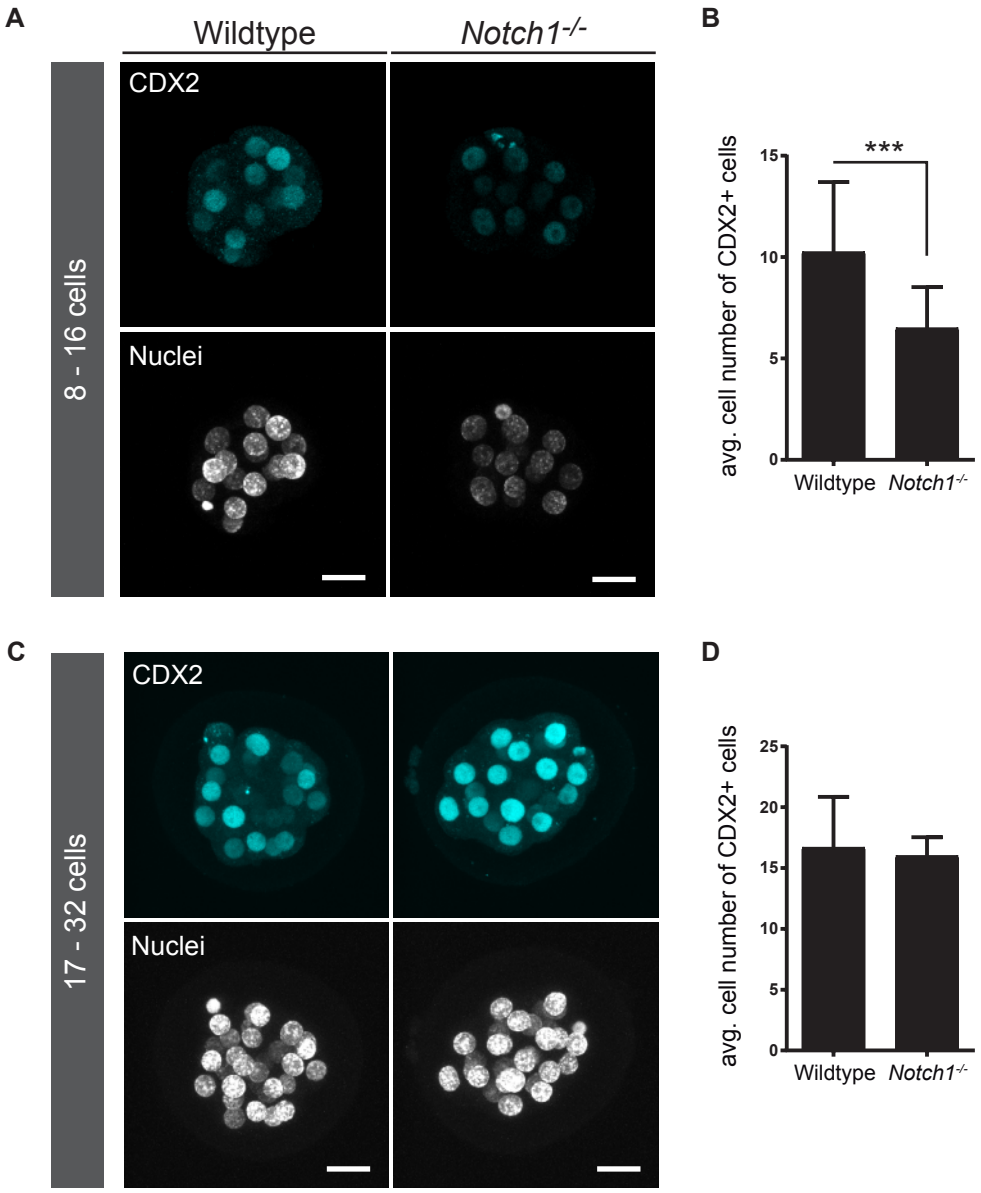

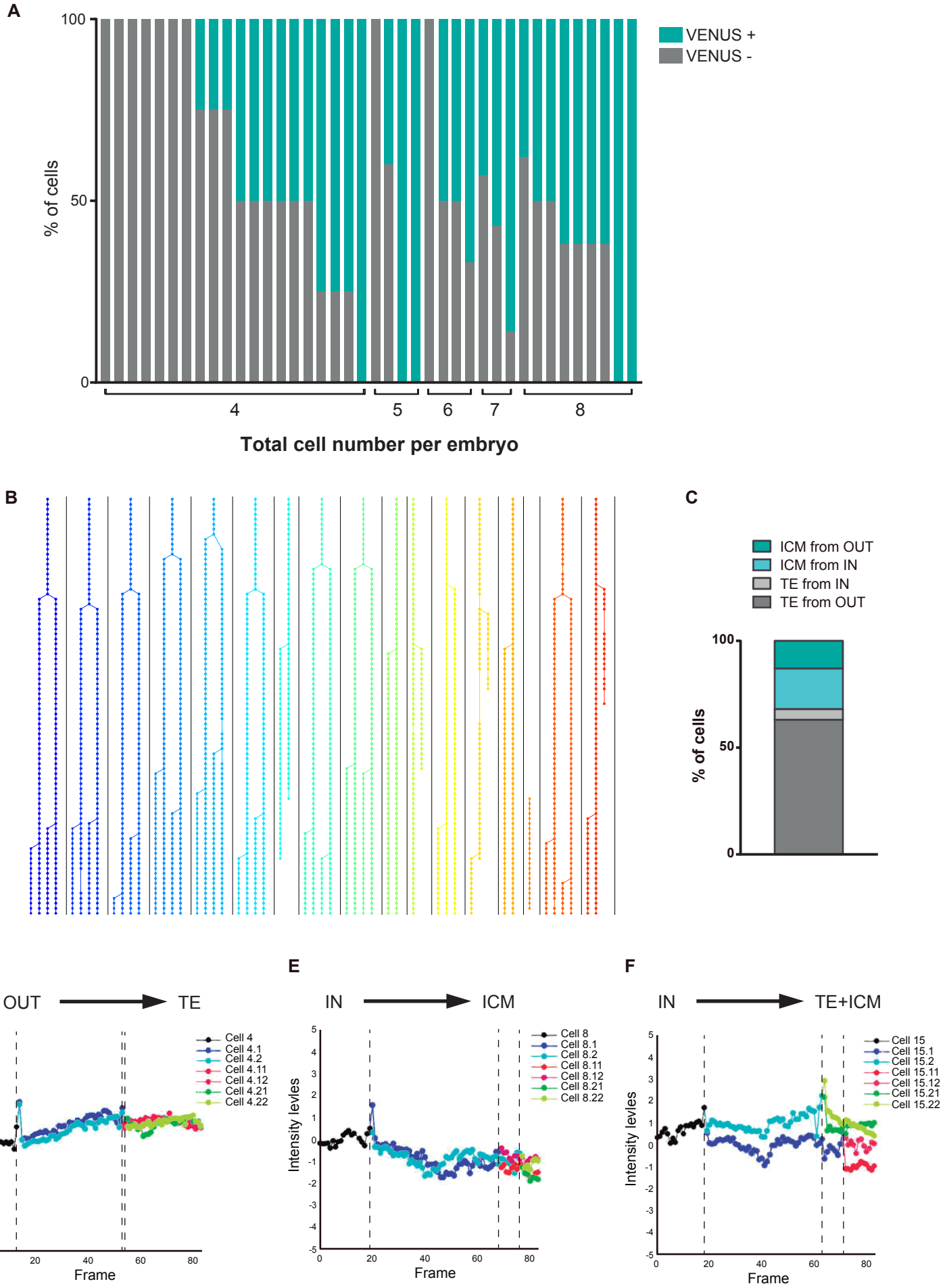

Menchero Fig S5